References

1. A.V. Aho and J.E. Hopcroft and J.D. Ullman, *Data Structures and Algorithms*, Addison-Wesley, 1987
2. G. Alefeld and J. Herzberger, *Introduction to Interval Computations*, Academic Press, 1983
3. V.M. Alekseev, Quasi-random oscillations and qualitative problems of celestial mechanics. In: *9th Mathematical school*, Kiev, 1972 (in Russian)
4. V.M. Alekseev, *Symbolic Dynamics, 11th Mathematical School*, Kiev, 1976 (in Russian)
5. A.A. Andronov and L.S. Pontryagin, Rough Systems, *Doklady Academy Nauk SSSR,* v.14, no.5, 247–250 (1937) (in Russian)
6. D. V. Anosov, *Geodesic flow on closed Riemannian manifold of negative curvature*, Trudy Math. Steclov Institute, v.90, 1967, 210 p., (in Russian)
7. N. Ampilova, K. Mot'kina, An algorithm for construction of the homotopic paths on a symbolic image, *The Fourth International Conference "Tools for Mathematical Modelling"*, St. Petersburg, 2003, book of abstracts, p. 160
8. J. Argyris, G. Faust, and M. Haase, *An Exploration of Chaos: An Introduction for Natural Scientists and Engineers*, Elsevier Science Ltd., 1994
9. L. Auslender and R. MacKenzie, *Introduction to Differentiable Manifolds*, N.Y., 1963
10. V. Avrutin, R. Lammert, M. Schanz, G. Wackenhut, and G. Osipenko, On the software package AnT 4.669 for the investigation of dynamical systems, *The Fourth International Conference "Tools for Mathematical Modelling"*, Mathematical Reaseach, v.9 (2003), 24–35, St. Petersburg State Polytechnic University, Russia
11. V. Avrutin and M. Schanz, Border-collision period-doubling scenario, *Phys. Rev. E*, v.70 (2004), 026222/1–11
12. N.P. Bhatia, G.P. Szego, *Stability theory of dynamical systems*, New York, Springer, 1970
13. G.D. Birkhoff, Nouvelles recherches sur les systemes dynamique, *Memoriae Pont. Acad. Novi Lincaei* v.3, no. 1(1935), 85–216
14. R. Bowen, *Equilibrium States and the Ergodic Theory of Anosov Diffeomorphisms, Lectures Note in Mathematics*, 470, Springer-Verlagh, N.Y., 1982
15. R. Bowen, *Symbolic Dynamics*, Ann. Math. Soc. Providence, R.I., vol.8, 1982

16. M. Brin, On incusion of diffeomorphism into flow, *Izvestiya VUZov,* no. 8(123), 1972, 19–25 (in Russian)
17. H. Broer, C. Simo, Hill's equation with quasi-periodic forcing: resonance tongues, instability pockets and global phenomena, *Bul. Soc. Bras. Mat.*, v.29 (1998), 253–293
18. I.U. Bronshtein, Theorem on structural stability of smooth extension of cascade, in *Algebraic invariants of dynamical systems, Mat. Issledovaniya,* v.67, Kishinev, Shtinisa, 12–29 (1980) (in Russian)
19. I.U. Bronshtein, *Nonautonomous dynamical system*, Kishinev, Shtinisa, 1984 (in Russian)
20. B.F. Bylov, R.E. Vinograd, D.M. Grobman, V.V. Nemytskii, *Theory of Lyapunov exponents*, Moscow, Nauka, 1966 (in Russian)
21. M.L. Cartwright and J.E. Littlewood, On non-linear differential equations of the second order, III, IV, *Acta Math.*, v.97 (1957), no. 3–4, 267–308; v.98 (1957), no 1–2, 1–110
22. T. Cormen, C. Leiserson, and R. Rivest, *Introduction to algorithms*, MIT Press, 2000
23. P. Cvitanović, Periodic orbits as the skeleton of classical and quantum chaos, *Physica D*, 51, 1991
24. P. Cvitanović. Focus issue on periodic orbit theory. *Chaos*, 2, 1992
25. F. Colonius and W. Kliemann, *The Morse spectrum of linear flows on vector bundles*, Trans. Amer. Math. Soc., 348, 4355–4388 (1996)
26. F. Colonius and W. Kliemann, *The Lyapunov spectrum of families of time varying matrices*, report 504, Inst. of Math. Augsburg Univ., 1994
27. F. Colonius and W. Kliemann, *The Dynamics of Control*, Burkhauser, 2000
28. C. Conley, Isolated Invariant set and the Morse Index, *CBMS Regional Conference Series*, v.38, Amer. Math. Soc., Providence, 1978
29. B. Coomes, H. Kocak, K. Palmer, Periodic shadowing, chaotic numerics, *Contemporary Mathematics*, 172, 1994
30. B. Coomes, H. Kocak, K. Palmer, Computation of long period orbits in chaotic dynamical systems, *Aust. Math. Soc. Gaz.*, v.24, no.5, 183–190 (1997)
31. M. Dellnitz, A. Hohmann, The computation of unstable manifolds using subdivision and continuation, in *Nonlinear Dynamical Systems and Chaos*, by Broer, H.W.; Gils, S.A. van; Hoveijn, I.; Takens, F. (eds.) PNLDE 19, Birkhauser, 449–459, 1996
32. M. Dellnitz, A. Hohmann, A subdivision algorithm for the computation of unstable manifolds and global attractors, *Numerische Mathematik* 75, 293–317, 1997
33. M. Dellnitz, O. Junge, An adaptive subdivision technique for the approximation of attractors and invariant measures, *Comput. Visual. Sci.* 1, 63–68, (1998)
34. M. Dellnitz, O. Junge, Almost invariant sets in Chuas circuit, *Int. J. Bif. and Chaos,* 7(11), 2475–2485, 1997
35. M. Dellnitz, G. Froyland, O. Junge, The algorithms behind GAIO – Set oriented numerical methods for dynamical systems, in *Ergodic Theories, Analysis, and Efficient Simulation of Dynamical Systems*, Springer, 2001, 145–175
36. M. Dellnitz and O. Junge, Set Oriented Numerical Methods for Dynamical Systems, in *Handbook of Dynamical Systems II: Towards Applications,* World Scientific, 2002, 221–264

37. R.L. Devaney, *An Introduction to Chaotic Dynamical Systems*, Addison-Wesley pub. com., 1990
38. P. Diamond, P. Kloeden, A. Pokrovskii, Cycles of spatial discretizations of shadowing dynamical systems, *Math. Nachr.*, v.171 (1995), 95–110
39. W. Dijkstra, A Note on two problems in connection with graphs, *Numerische Math.*, v.1 (1959), 269–271
40. M.J. Feigenbaum, The Universal Metric Properties of Nonlinear Transformations, *J. Stat. Phys.*, v.21, no. 6 (1979), 669–707
41. M.J. Feigenbaum, Quantitative Universality for a Class of Nonlinear Transformations, *J. Stat. Phys.*, v.19, no. 1 (1978), 25–53
42. J. Franke and J. Selgrade, Hyperbolicity and chain recurrence, *J. Differential Equations,* 26 (1977), 27–36
43. G. Froyland, O. Junge, G. Ochs, Rigorous computation of topological entropy with respect to finite partition, Web-article, URL: *http://www.math.uni-paderborn.de/agdellnitz/papers/topen15.ps.gz*
44. D. Fundinger, T. Lindström, G. Osipenko, On the appearance of multiple attractors in discrete food-chains, submitted in *Applied Mathematics and Computation*, 2006
45. N.K. Gavrilov and L.P. Silnikov, On three-dimansional dynamical systems close to systems with a structurally unstable homoclinic curve, *Math. USSR Sb.*, v.88 (1972), 467–485; v.90 (1973), 139–156
46. G. Golub, C. Van Loan, *Matrix computations*, Mir, Moscow, 1999
47. A. Gragnami, O. De Feo, and S. Rinaldi, Food chains in the chemostat: Relationships between mean yield and complex dynamics, *Bulletin of Math. Biology*, v.60, 703–719, 1998
48. J. Guckenheimer, P. Holmes, *Nonlinear Oscilations, Dynamical Systems and Bifurcations of Vector Fields,* Springer-Verlag, N.Y., 1983
49. B. Hao and W. Zheng, *Applied Symbolic Dynamics and Chaos*, World Scientific, Singapore, 1998
50. J. Hadamard, Les surfaces a courbures opposees et leurs lignes geodesiques, *Journal de Matematiques Pure et Applique,* v.4 (1898), 27–73
51. P. Hartman, *Ordinary Differential Equations*, N.Y., 1964
52. M.E. Henderson, Computing invariant manifolds by integrating fat trajectories, *IBM Research, Technical Report RC22944*, 2003
53. M. Henon, A two-dimensional mapping with strange attractor. *Copmm. Math. Phys.*, 50, 1976, 69–77
54. M. Hirsch and S. Smale, *Differential Equations, Dynamical Systems and Linear Algebra,* N.Y. 1970
55. D. Hobson, An efficient method for computing invariant manifolds, *J. Comput. Phys.*, v.104 (1991), 14–22
56. S.L. Hruska, Constructing an expanding metric for dynamical systems in one complex variable, *Nonlinearity*, v.18 (2005), 81–100
57. C.S. Hsu, *Cell-to-Cell Mapping.* Springer-Verlag, N.Y., 1987
58. F. Hunt, Unique ergodicity and the approximation of attractors and their invariant measures using Ulam's method, *Nonlinearity*, v.11, no. 2, 307–317 (1998)
59. M. Hurley, Chain recurrence and attraction in non-compact spaces, *Ergodic Theory and Dynamical Systems*, 11 (1991), 709–729
60. K. Ikeda, Multiple-valued stationary state and its instability of the transmitted light by a ring cavity system, *Opt. Commun.*, 30, 257–261, 1979

61. A. Jorba, and C. Simo, On quasiperiodic perturbation of elliptic equilibrium points, *SIAM J. of Math. Anal.*, 27 (1996), 1704–1737
62. O. Junge, Rigorous discretization of subdivision techniques, in *Proceedings of Equadiff '99*, Berlin, 2000
63. T. Kaczynsky, K. Mishaikow, M. Mrozek, *Computation homology,* Applied mathematic sciences, 157, Springer, N-Y, 2004
64. K. Kaneko (editor), *Theory and Applications of Coupled Map Lattices,* Wiley, New York, 1993
65. S. Khryashchev, *On local controllability along trajectories,* VINITI, 868-B 97, 1997, 1–14
66. S.Yu. Kobjakov, D.Yu. Matiassevich, G.S. Osipenko, Location of the invariant sets. *Proceedings of the Fourth International Conference Tools for Mathematical Modelling*, Saint-Petersburg State Polytechnic University, 2003, 300–3007
67. A.N. Kolmogorov, S.W. Fomin, *An elements of the theory of functions and the functional analysis,* Science, Moscow, 1968 (in Russian)
68. A.N. Kolmogorov, New mesure invariant for transitive dynamical systems and endomorphisms of Lebesgue spaces, *Doklady AN USSR,* 115, no. 5 (1958), 861–864
69. B. Krauskopf, H.M. Osinga, Globalizing two-dimensional unstable manifolds of maps, *Int. J. Bifurcation and Chaos*, v.8, no. 3 (1998), 483–503
70. B. Krauskopf, H.M. Osinga, E.J. Doedel, M.E. Henderson, J. Guckenheimer, A. Vladimirsky, M. Dellnitz, O. Junge, A survey of methods for computing (un)stable manifolds of vector fields, *Int. J. Bifurcation and Chaos*, v.15, no. 3 (2005)
71. B.Yu. Levit and V.N. Livshits, *Nonlinear Network Transport Problems* Moscow, Transport, 1972 (in Russian)
72. D. Lind, B. Marcus, *An introduction to symbolic dynamics and coding,* New York, 1995
73. T. Lindström, On the dynamics of discrete food chains: Low- and high-frequency behavior and optimality of chaos, *Journal of Mathematical Biology*, v.45 (2002), 396–418
74. E.N. Lorenz, Deterministic nonperiodic flow, *J. Atmos. Sci.*, 20:130–141, 1963
75. A.M. Lyapunov, *Probleme General de la Stabilite an Mouvement*, Kharkov, 1892
76. G.G. Malinetskii, A.V. Potapov, A.I. Rakhmatov, E.B. Rodichev, Limination of delay reconstruction for chaotic systems with board spectrum, *Phys. Lett. A.*, v.179, 15, 1993
77. G.G. Malinetskii, A.V. Potapov, A.I. Rakhmatov, Limination of delay reconstruction for chaotic systems with board spectrum, *Phys. Rev. E.*, v.48, 904–912, 1993
78. G.G. Malinetskii, A.V. Potapov, *Modern problems in nonlinear dynamics*, Moscow, 2000 (in Russian)
79. R. Mane, Characterizations of AS diffeomorphisms, *Lect. Notes Math.*, v.597, 389–394 (1977)
80. R. Mane, A proof of the C^1 stability conjecture, *Publ. Math., Inst. Hautes Etud. Sci.*, 66, 161–210 (1988)
81. D.Yu. Matiyasevich, Localization of Invariant Sets of Dynamical Systems, *Journal of Mathematical Sciences*, v.124 (2004), no. 3, 4990–5000

82. D.Yu. Matiyasevich, E.I. Petrenko, Algorithms for the construction of isolated invariant subsets of the symbolic image, *Proceedimgs of XXXVI conference "Control Processes and Stability",* St.Petersburg, 2005, 341–347
83. J.R. Miller and J.A. Yorke, Finding all periodic orbits of maps using newton methods: Sizes of Basins, *Physica D*, 135: 195–211, 2000
84. K. Mischaikow, Topological techniques for efficient rigorous computations in dynamics, *Acta Numerica*, 2002
85. D.A. Mizin, *Algorithms based on applied symbolic dynamics,* PhD dissertation, St. Petersburg State Polytechnic University, 2002 (in Russian)
86. D.A. Mizin, G. Osipenko, S. Kobyakov, The estimats for the topological entropy of the dynamic system, *Proceedings of the third international conference "Tools for mathematical modelling"*, 2001, 85–105
87. A.A. Moiseev, Symbolic image od dynamical system and algorithms for investigation, *Differential Equations and applications,* abstracts of the International Conference, St. Petersburg, 1996, 152–153
88. R. Montgomery, The N-body problem, the briad group, and action-minimizing periodic solutions, *Nonlinearity*, v.11 (1998), 363–376
89. M. Morse, A one-to-one representation of geodesics on a surface of negative curvature, *Amer. J. Math.*, v.43 (1921), no. 1, p.33–51
90. M. Morse, G.A. Hedlund, Symbolic dynamics I, II *Amer. J. Math.*, v.60 (1938), no. 4, p.815–866; v.62 (1940), no 1, p.1–42
91. S.E. Newhouse, Diffeomorphisms with infinitely many sinks, *Topology,* v.13, 1974, 9–18
92. Z. Nitecki, *Differentiable Dynamics.* London, 1971
93. Z. Nitecki and M. Shub, Filtrations, decompositions, and explosions, *Amer. J. of Math.*, v.97 (1975), no.4, 1029–1047
94. H.E. Nusse, J.A. Yorke, *Dynamics: Numerical Explorations,* Springer-Verlag, 1997
95. G.S. Osipenko, On a symbolic image of dynamical system, in *Boundary value problems*, Perm, 1983, 101–105 (in Russian)
96. G.S. Osipenko, Verification of the transversality condition by the symbolic-dynamical methods, *Differential Equations*, v.26, N9, 1126–1132; translated from *Differentsial'nye Uravneniya*, v.26, N9, 1528–1536, 1990
97. G.S. Osipenko, The periodic points and symbolic dynamics, in *Seminar on Dynamical Systems. Euler International Mathematical Institute, St. Petersburg, Russia, October and November, 1991*, Birkhauser Verlag, Basel, Prog. Nonlinear Differ. Equ. Appl. 12, 261–267 (1993)
98. G.S. Osipenko, Localization of the chain recurrent set by symbolic dynamics methods, *Proceedings of Dynamics Systems and Applications*, v.1, (1994), 227–282, Dynamic Publishers Inc
99. G. Osipenko and I. Komarchev, Applied symbolic dynamics: construction of periodic trajectories, *WSSIAA*, 4(1995), 573–587
100. G. Osipenko and I.Il'in, Methods of Applied Symbolic Dynamics, *Proceedings of Dynamics Systems and Applications*, v.2 (1996), 451–160
101. G. Osipenko, Indestructibility of invariant locally non-unique manifolds, *Discrete and Continuous Dynamical Systems*, v.2, no.2 (1996), 203–220
102. G. Osipenko, E. Ershov and J. Kim, *Lectures on Invariant Manifolds of Perturbed Differential Equations and Linearization*, St. Petersburg Polytech. University, 1996

103. G. Osipenko and Eu. Ershov, Perturbation of invariant manifolds of ordinary differential equations, in *Six lectures on dynamical systems,* editors B. Aulbach and F. Colonius, Wold Scientific, Singapore, 1996
104. G. Osipenko, Morse Spectrum of Dynamical Systems and Symbolic Dynamics, *Proceedings of 15th IMACS World Congress*, v.1 (1997), 25–30
105. G. Osipenko, Linearization near a locally non-unique invariant manifold, *Discrete and Continuous Dynamical Systems*, v.3, no.2 (1997), 189–205
106. G. Osipenko and S. Campbell, Applied Symbolic Dynamics: Attractors and Filtrations, *Discrete and Continuous Dynamical Systems,* v.5, no.1&2, 43–60 (1999)
107. G. Osipenko, Spectrum of a Dynamical System and Applied Symbolic Dynamics, *Journal of Mathematical Analysis and Applications*, v.252, no. 2, 587–616 (2000)
108. G.S. Osipenko, J.V. Romanovsky, N.B. Ampilova, E.I. Petrenko, Computation of the Morse Spectrum, *Journal of Mathematical Sciences*, v.120, no. 2 (2004), 1155–1166
109. G.S. Osipenko, *Lectures on symbolic analysis of dynamical systems*, St. Petersburg State Polytechnic University, 2004
110. J. Palis, J. Melo, *Geometric Theory of Dynamical Systems,* Springer-Verlag, New York (1982)
111. P. Pilarczyk, Computer assisted method for proving existence of periodic orbits. *TMNA*, 13(2): 365–377, 1999
112. P. Pilarczyk, Homology software, in *Computational homology program*, http:www.gatech.edu/chom
113. S.Yu. Pilyugin, *The space of Dynamical Systems with C^0-Topology*, Springer-Verlag, 1994, Lec. Notes in Math., 1571, 180p
114. S. Pissanetzky *Sparse Matrix Technology*, New York, Academic Press, 1984
115. V.A. Pliss, *Integral Sets of Periodic System of Differential Equations*, Moscow, 1977 (in Russian)
116. H. Poincare, Sur le probleme des trois corps et les equations de la dynamique, *Acta Mathematica* v.13 (1890), 1–271
117. H. Poincare, *Les methodes nouvelles de la mecanique celeste,* I–III (1892–1899), Gauthiers-Villars
118. J. Robbin, A structural stability theorem, *Annals of Math.*, v.94, no.3, 447–493 (1971)
119. C. Robinson, Structural stability of C^1-diffeomorphism, *J. Diff. Equat.*, v.22, no.1, 28–73 (1976)
120. C. Robinson, *Dynamical Systems: Stability, Symbolic Dynamics and Chaos*, 1995
121. Yu.V. Romanovsky, Optimization and stationary control of discrete deterministic process in dynamic programming *Kibernetika* **2**, 66–78 (in Russian); Engl. transl. *Cybernetics* **3**, 1967
122. M.L. Rosenzweig, Exploitation in three throphic levels, *The American Naturalist,* 107 (954), 275–294, 1973
123. R. Sacker and G. Sell, Existence of dichotomies and invariant splitting for linear differential systems I-III, *J. Diff. Eq.* v.15, no3 (1974), 429–458, v.22, no.2 (1976) 476–522
124. R. Sacker and G. Sell, A spectral theory for liner differential systems, *J. Diff. Eq.*, v.27, no. 3, (1978), 320–358

125. D. Salamon and E. Zehnder, Flows on vector bundles and hyperbolic sets, *Trans. Amer. Math. Soc.*, v.306, no. 2 (1988), 623–649
126. J. Selgrade, Isolated invariant sets for flows on vector bundles, *Trans. Amer. Math. Soc.*, v.203 (1975), 359–390
127. G. Sell, Nonautonomous differential equations and topological dynamics, *Trans. AMS*, 127 (1967), 241–283
128. R. Sedgewick, *Algorithms in Modula 3*, Addison-Wesley, Massachusetts, 1993
129. A.N. Sharkovsky, Structure theory of differentiable dynamical systems and weak nonwandering points, *Abh. Akad. Wiss. DDR. Abt. Math. Naturwiss. Techn.*, v.4 (1977), 193–200
130. A.N. Sharkovsky, Yu.L. Maistrenko, E.Yu. Romanenko, *Diffenrence equations and applications,* Naukova dumka, Kyev, 1986 (in Russian)
131. M. Shub, Stabilite globale de systems denamiques, *Asterisque*, v.56 (1978), 1–21
132. L.P. Silnikov, A case of the existence of a denumerable set of periodic motions, *Sov. Math. Dokl.,* v.6 (1965), 163–166
133. L.P. Silnikov, A contridution to the problem of the structure of an extended neighborhood of a rough state of saddle-focus type, *Math. USSR Sb.,* v.10 (1970), 91–102
134. C. Simo, Effective computations in hamiltonian dynamics, in *Cent ans apes les Methodes Nouvelles de H. Poincare*, 1–23, 1996
135. C. Simo, Invariant curves of analytic perturbed nontwist area preserving maps, *Regular and Chaotic Dynamics*, v.3 (1998), no. 3, 180–195
136. S. Smale, Diffeomorphisms with many periodic points, in *Differential and Combinatorial Topology*, Princeton Univ., 1965, 63–80
137. S. Smale, Differentiable dynamical systems, *Bull. Amer. Math. Soc.,* 73, 1967
138. S. Smale, The $\Omega-$ stability theorem, in *Global Analysis, Proc. Symp. in Pure Math.*, v.XIV, Amer. Math. Soc. 1970
139. C. Sparrow, *The Lorenz Equations: Bifurcations, Chaos, and Strange Attractors*, Springer, N.Y., 1973
140. H.J. Sussmann, Some properties of vector fields systems witch are not altered by small perturbations, *J. Differential Equations*, v.20 (1976), no. 2, 292–315
141. R. Tarjan, Depth-First Search and Linear Graph Algorithms, *SIAM J. Comput*, v.1 (1972), 146–160
142. R. Tarjan, *Data structures and network algorithms*, Philadelphia, Pa., 1991
143. H. Whitney, Diferentiable Manifolds, *Ann. Math.*, 37 (1936), pp. 645–680
144. S. Wiggins, *Introduction to Applied non linear Dynamical Systems and Chaos*, 1990
145. A. Wolf, J. Swift, H. Swinney and J. Vastano, Determining Lyapunov exponents from a time series, *Physica D,* 16 (1985), 285–317
146. Z. You, E.J. Kostelich, J.A.Yorke, Calculating stable and unstable manifolds, *Internat. J. Bifur. Chaos Appl. Sci. Engrg.*, v.1, no. 3, (1991), 605–623
147. Zh.T. Zhusubaliyev and E. Mosekilde, Bifurcations and chaos in piecewise-smooth dynamical systems, v.44, *Nonlinear Science A*, New Jersey, 2003

A

Double Logistic Map

Ampilova N.B.

St. Petersburg State University, Dept. Comp. Science
Russia

nataly@is1483.spb.edu

A.1 Introduction

Consider the map $T = T_{\lambda,\mu}$ of extended plane $\tilde{\mathbb{R}}^2 = \mathbb{R}^2 \cup \infty$ into itself: $z_{n+1} = T(z_n), z = (x, y)$, where T has the form

$$T : \quad \begin{array}{l} x_1 = (1-\lambda)\, x + \lambda\mu y(1-y), \\ y_1 = (1-\lambda)\, y + \lambda\mu x(1-x), \end{array} \tag{A.1}$$

and λ, μ — are real parameters.

The topology on $\tilde{\mathbb{R}}^2$ is supposed to be induced by the Riemann sphere topology, namely, various neighbourhoods of the point at infinity are the complements of all possible compacts. We assume that ∞ is fixed point. The dynamical system generated by the map (A.1) was studied in [1,6]. The estimate of the domain of attraction to the point at infinity was obtained. Among other things it was proved that the outside of the disk

$$(x-r)^2 + (y-r)^2 \le 2r^2, \tag{A.2}$$

where $r = 0.5(1-\lambda+\lambda\mu)/\lambda\mu)$, is a neighbourhood of that point.

The map (A.1) has 4 fixed points: $O_0(0,0)$, $O_1(1-\frac{1}{\mu}, 1-\frac{1}{\mu})$ lying on the diagonal $y = x$, and $O_2(t,u)$, $O_3(u,t)$, where

$$t = \frac{1+\mu-\sqrt{(\mu-1)^2-4}}{2\mu}, \qquad u = \frac{1+\mu+\sqrt{(\mu-1)^2-4}}{2\mu}. \tag{A.3}$$

The point O_0 is saddle for $\lambda \in (0, \frac{2}{\mu+1})$ and unstable node for $\lambda \geq \frac{2}{\mu+1}$.

Similarly, O_1 is saddle for $\lambda \in (0, \frac{2}{\mu-1})$ and unstable node for $\lambda \geq \frac{2}{\mu-1}$.

The fixed points O_2 and O_3 have eigenvalues s_1, s_2 equal to $1 - \lambda \pm \lambda i\sqrt{(\mu-1)^2 - 5}$, so they are focuses for $\mu \geq 1 + \sqrt{5}$ or $\mu \leq 1 - \sqrt{5}$ and nodes elsewise.

We explore the map in the focus O_2 neighbourhood and consider the conditions of appearance an invariant curve and periodic orbits in its vicinity.

A.2 Hopf Bifurcation

It is known that under some assumptions a bifurcation of a fixed point when it is focus leads to the occurence of an invariant circle which is smooth for parameters values in a neighborhood of the bifurcation point. The fixed point changes its stability type when the absolute value of the eigenvalue of Jacobi matrix in this point crosses a unit circle. Let the point on the unit circle be $s_0 = e^{i2\pi p/q}$, with (p, q) in lowest terms. It is said that p/q resonance occurs on the invariant circle if there is a pair of periodic orbits, one consisting of saddles and the other of sinks, which rotation number is p/q.

The case $q \geq 5$ is called weak resonance. An infinite number of periodic orbits are created and destroyed on the circle immediately after the Hopf bifurcation. Given p/q, a pair of periodic orbits exists on the invariant circle for parameters values lying in the narrow cusped region ("resonance horn" or "Arnold tongue") [5]. By Arnold's method this horn can be constructed by analytical methods. Unfortunately, such an approach is valued only for parameter when the invariant circle is smooth. In other case we need a computer simulation.

The strong resonance, $q = 1, 2, 3, 4$ exhibits rather different behaviour, the details of which are not yet fully understood. In this situation Arnold's method is not applicable as well. The articles [5, 7] are devoted to detailed investigation of Hopf bifurcation for two-parametric families of plane maps. We applied a combined approach to the map (A.1). It has been shown that a transition to chaotic regime in the case of strong resonance is a result of recurring Hopf bifurcation.

Arnold's method for two-parameter families of plane maps.
V. Arnold suggested using the following scheme to investigate such families. A map $\mathbb{R}^2 \to \mathbb{R}^2$ can be written as a function of one complex variable, and two real parameters can be written as a single complex parameter. Consider a map

$$z \to f_\mu(z) = \mu z + O(|z|^2), \tag{A.4}$$

where μ is a complex parameter.

Note that $z = 0$ is a fixed point of f_μ for all μ. The eigenvalues at this fixed point are μ and $\bar{\mu}$.

It should be noted that almost any two-parameter family of maps having a fixed point with complex eigenvalues can be transformed to the form (A.4) as follows. First translate the fixed point to the origin. Then make a complex linear change of coordinates which diagonalizes the linear part of the map. Finally, introduce the eigenvalue at the origin as a new complex parameter. It is necessary that the function which gives this eigenvalue in terms of the original parameters should be invertible.

Thus, the fixed point $z = 0$ is stable for $|\mu| < 1$ and unstable for $|\mu| > 1$. To study the bifurcation occuring for $|\mu| = 1$ (loss of stability), consider the point μ_0 on the unit circle. We assume that $\mu_0^k \neq 1, k = 1, 2, 3, 4$ and write f_μ in its normal form

$$f_\mu(z) = \mu z + c(\mu)z|z|^2 + O(|z|^4). \tag{A.5}$$

Let $Re(\bar{\mu_0}c(\mu_0)) < 0$. Then under these assumptions, the Hopf bifurcation theorem [4] states, that for μ near μ_0 with $|\mu| > 1$ the map f_μ has an attracting invariant circle surrounding $z = 0$. Moreover, the areas of existence of periodic orbits ("resonance horns") may be constructed by analytical methods.

Numerical methods of investigation for two-parameter families of plane maps.
Arnold's method is valued only in the case of weak resonance for parameter values when the invariant circle is smooth. Hence to extend a resonance horn into the parameter area where the circle losses continuity we need a computer simulation. Given in [5] numerical method of construction of resonance horns is based on the following scheme.

When the parameter is outside the horn, no periodic point of rotation number p/q is present. When the parameter encounters the boundary of the horn, q saddle-nodes appear on the invariant circle. As the parameter passes into the interior of the horn, the saddle-nodes bifurcate forming saddle-sink pairs. There are now two periodic orbits on the invariant circle, one consisting of saddles and the other of sinks. The q^{th} iterate of the map has $2q$ fixed points, alternating between saddles and sinks around the invariant circle. As the parameter continues to move across the horn, the saddles and sinks move apart. As the parameter approaches the other boundary, these points form different saddle-sink pairs. When the parameter approaches another boundary of the horn, these new saddle-sink pairs combine to form saddle-nodes.

Consider a two-parameter family of plane maps $F_{a,b}$. Given a, b and a number q, to find a q-periodic orbit of the map means to solve the equation $F^q(z) = z$, where $z = (x, y)$. Let z_0 be a solution of this equation. If the determined orbit is saddle or sink, then the point (a, b) is in the resonance horn. If there is 1 among eigenvalues of $DF^q(z_0)$, then z_0 is a periodic saddle-node and the point (a, b) lies on the boundary of the resonance horn. These boundary points are computed using Newton's method to solve the system equations: the above equation and the condition that 1 is an eigenvalue of the periodic point.

When the eigenvalue of the Jacobi matrix of the mapping F^q in the fixed point has absolute value 1, we can write it in the form

$$e^{i2\pi p/q} = cos2\pi p/q + isin2\pi p/q = u(a,b) + iv(a,b).$$

That allows to detail a point on the unit circle where a resonance horn starts to grow from.

For a case of strong resonance we apply a computer simulation and Newton's method to find periodic orbits and determine "horns".

A.2.1 The Application to Double Logistic Map

For the case of the focus O_2 these eigenvalues when crossing the unit circle can be written as $|s_1| = (1-\lambda)^2 + \lambda^2(\mu^2 - 2\mu - 4)$ and

$$|s_1| = 1 \Longleftrightarrow \lambda(\lambda(\mu^2 - 2\mu - 3) - 2) = 0.$$

As $\lambda > 0$, we have

$$(\mu - 1)^2 = 4 + \frac{2}{\lambda}. \tag{A.6}$$

This relation determines a line (Hopf bifurcation line) on the plane of parameters (λ, μ) such that for $1 + \sqrt{5} \leq \mu \leq 1 + \sqrt{4 + \frac{2}{\lambda}}$ the focuces O_2, O_3 are stable. When $\mu = 1 + \sqrt{4 + \frac{2}{\lambda}}$ an invariant curve appears in a O_2 (O_3) neighborhood, which is destroyed under the parameters changing.

In [2] the values of the parameter λ corresponding to an occurence of invariant curve were obtained by computer simulation methods. Let a point (λ_0, μ_0) is on the Hopf bifurcation line. Changing λ from λ_0 by a step ε, we can find the parameter λ value when an invariant curve occurs(λ_b) and is destroyed (λ_e). The obtained data are shown in Table A.1. It should be noted that the conditions $\mu \geq 1 + \sqrt{5}$ and $(\mu - 1)^2 \leq 4 + \frac{2}{\lambda}$ are satisfied simultaneously for $\lambda \leq 2$.

The following periodic orbits (weak resonance) were obtained by approximative method and specification using Newton's method:

$$\lambda = 0.512603, \mu = 4.11,\ p/q = 1/7; \lambda = 0.55260, \mu = 4.11,\ p/q = 3/22.$$

As for $p/q = 1/7$ we have $\cos\frac{2\pi}{7} = 1 - \lambda$ hence $1 - \lambda \approx 0.6239$ and $\lambda \approx 0.3761$. So, 1/7-resonance occurs from the bifurcation line $\mu = 1 + \sqrt{4 + \frac{2}{\lambda}}$ when $\lambda \approx 0.3761$ and $\mu \approx 4.052$. After the destroying of the invariant curve the periodic orbit with $p/q = 2/15$ was found for $\lambda = 0.57260, \mu = 4.11$. The case of strong resonance means that $q \in \{1, 2, 3, 4\}$ and $(p, q) = 1$. Hence $p/q \in \{1, 1/2, 1/3, 1/4, 2/3, 3/4\}$. The correspondence between p/q, λ and μ is given in the following table.

Table A.1.

μ	$\lambda = \frac{2}{(\mu-1)^2-4}$	$(\lambda_b(\mu), \lambda_e(\mu))$	μ	$\lambda = \frac{2}{(\mu-1)^2-4}$	$(\lambda_b(\mu), \lambda_e(\mu))$
3.41	1.10613	1.11–1.2	3.56	0.783	0.797–0.905
3.42	1.07735	1.078–1.193	3.57	0.767	0.781–0.87
3.43	1.04992	1.061–1.15	3.58	0.75	0.79–0.86
3.44	1.02375	1.036–1.139	3.59	0.738	0.752–0.85
3.45	0.99875	1.011–1.13	3.6	0.724	0.739–0.85
3.46	0.9748	0.986–1.12	3.7	0.607	0.624–0.7
3.47	0.9519	0.966–1.08	3.8	0.52	0.536–0.667
3.48	0.93	0.945–1.05	3.9	0.4535	0.47–0.61
3.49	0.909	0.92–0.98	4.0	0.4	0.41–0.55
3.50	0.888	0.9–0.97	4.1	0.356	0.38–0.5
3.51	0.869	0.88–0.96	4.2	0.32	0.34–0.47
3.52	0.85	0.86–0.95	4.5	0.242	0.263–0.4
3.53	0.83	0.846–0.95	4.6	0.223	0.24–0.32
3.54	0.815	0.829–0.94	4.7	0.2	0.22–0.3
3.55	0.799	0.812–0.92	4.8	0.191	0.21–0.29

p/q	1	1/2	1/3	1/4	2/3	3/4
λ	0	2	3/2	1	3/2	1
μ	$\forall$	$1+\sqrt{5}$	$1+4\sqrt{3}/3$	$1+\sqrt{6}$	$1+4\sqrt{3}/3$	$1+\sqrt{6}$

Since the case of $p/q = 1(\lambda = 0)$ is singular and the fixed point O_2 is focus for $\lambda \leq 2$, we investigate the cases when $\lambda = 1$ and $\lambda = 3/2$.

$\lambda = \mathbf{1}$.

On the bifurcation line (A.6) it corresponds to $\mu = 1 + \sqrt{6}$. The eigenvalue is equal $\pm i$ and $e^{i\alpha} = \cos\alpha + i\sin\alpha$, so $\alpha = \pi/2$ and $e^{i\pi/2} = e^{2\pi i/4}$, i.e. $p/q = 1/4$. Nevertheless, there are no 4-periodic orbits in this case. The following periodic orbits were found:

$$\lambda = 1.14,\ \mu = 3.44,\ p/q = 1/11;$$

$$\lambda = 1.16,\ \mu = 3.44,\ p/q = 1/17;$$

$$\lambda = 1.18,\ \mu = 3.44,\ p/q = 1/7.$$

The behaviour of trajectories in a neighborhood of the invariant curve is shown in Fig. A.1–A.2. Fig. A.1 shows an appearance of the invariant curve and its deformation. Fig. A.2 illustrates recurrent Hopf bifurcation and, as a consequence, transition to chaotic regime.

$\lambda = \mathbf{3/2}$.

In this case the situation is more complicated. The eigenvalue is equal $-1/2 + i\sqrt{3}/2$ and $q = 3$. Computer simulation shows the existence of a 3-periodic

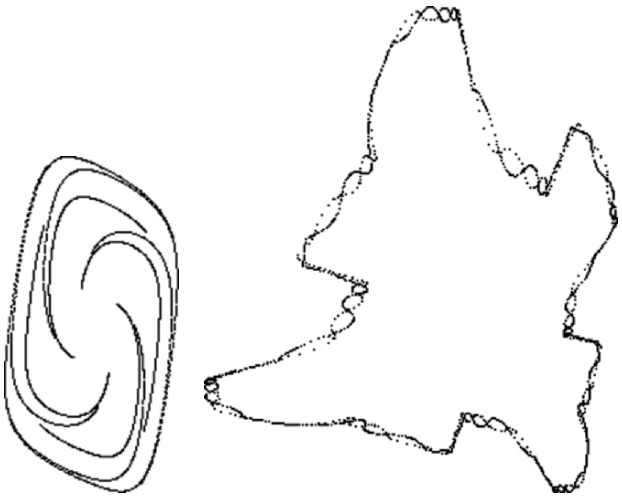

Fig. A.1. Strong resonance for the map (A.1): appearance of the invariant curve for $\lambda = 1.002,\ \mu = 3.44949;\ x \in [0.825, 0.865]$, $y \in [0.41, 0.46]$ and its deformation for $\lambda = 1.144,\ \mu = 3.44949;\ x \in [0.8, 0.9]$, $y \in [0.32, 0.56]$

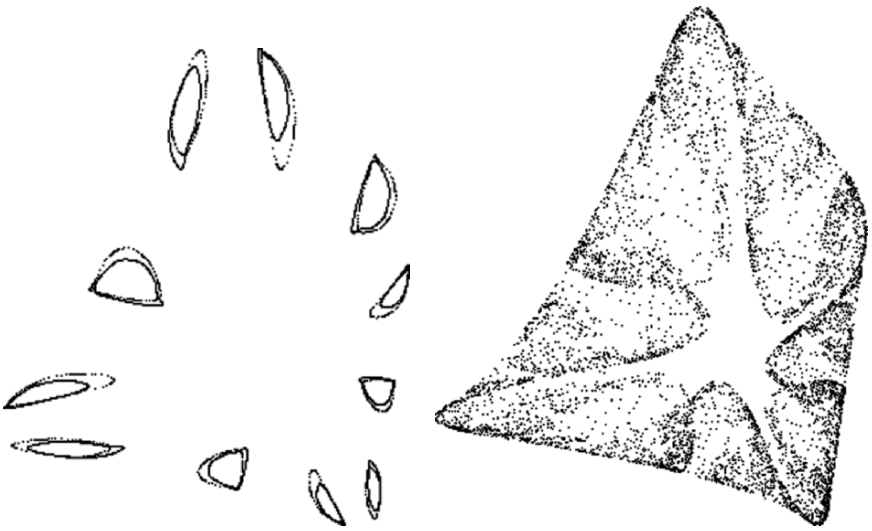

Fig. A.2. Strong resonance for the map (A.1): recurrent Hopf bifurcation for $\lambda = 1.147,\ \mu = 3.44949;\ x \in [0.8, 0.9]$, $y \in [0.32, 0.56]$ and the transition to chaotic regime for $\lambda = 1.162,\ \mu = 3.44949;\ x \in [0.8, 0.9]$, $y \in [0.32, 0.56]$

orbit: Fig. A.3 demonstrates a set, arizing in a vicinity of the focus O_2 and its detailed part, Fig. A.4 also illustrates this part for different values of the parameter λ. It should be noted that this structure arises for $\lambda < 3/2 (\approx 1.49)$ and persists with some modifications up to $\lambda \approx 1.50080$.

Fig. A.3. Strong resonance for the map (A.1), case $\lambda = 3/2$. The appearance of 3-periodic saddle orbit for $\lambda = 1.4938,\ \mu = 3.3094;\ x \in [0.7, 0.85]$, $y \in [0.3, 0.62]$ and the magnified middle part of the picture for $\lambda = 1.4941,\ \mu = 3.3094;\ x \in [0.8, 0.85]$, $y \in [0.4, 0.5]$

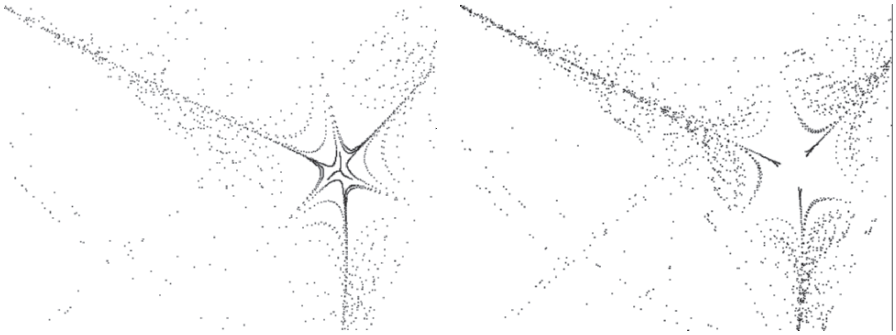

Fig. A.4. Strong resonance for the map (A.1), case $\lambda = 3/2$. The phase portrait in a vicinity of 3-periodic oprbit for $\lambda = 1.4955,\ \mu = 3.3094;\ x \in [0.81, 0.83]$, $y \in [0.44, 0.5]$ and for $\lambda = 1.4956,\ \mu = 3.44949;\ x \in [0.81, 0.83]$, $y \in [0.44, 0.5]$

A.3 Construction of Periodic Orbits

As was mentioned in the previous section, methods of computer simulation were applied to investigate the complex behaviour of the map in a vicinity of the invariant curve for Hopf bifurcation. λ, μ, for which an invariant curve occurs in the focus vicinity was obtained. In particular, it was shown that for $\lambda = 0.512603$, $\mu = 4.11$ the 7-periodic orbits appear. The numerical method

of the construction of a periodic orbit is a construction of an initial approximation of the periodic orbit and its following refinement by Newton's method.

A.3.1 Construction of the First Approximation

The following methods were applied to find an initial approximation of a periodic orbit:

1. Methods of symbolic dynamics.
   For the system under investigation its symbolic image is considered. It is known that periodic paths on the symbolic image correspond to periodic orbits of the system. So, we apply a method of the search of periodic orbits with given period on a graph.
2. Lattice method.
   A lattice with a step h is constructed on the set defined by the inequality (A.2). Then the condition $||(T^k(z) - z)|| < \varepsilon$, where k is a given period and $\varepsilon \geq h$, is verified for every point z of the lattice. The points of the lattice for which the above condition is fulfilled are the points of the first approximation. Denote by P the set of such points. The value of ε is chosen to satisfy the condition $\varepsilon \geq h$. The sets P consructed for $\varepsilon = 0.01228$ and $\varepsilon = 0.06$ are shown in Fig. A.5. The circle shows a boundary for the invariant set of the system, the dark background displays the invariant set and blank squares depict the fixed points. The areas filled by the black color show the sets P.

The set P contains the first approximations to the roots of the equation $T^k(z) - z = 0$. To refine the roots we apply Newton's method, namely Theorem 25. In our problem $F(z_0) = T^k(z_0) - z_0$ and $DF(z_0) = DT^k(z_0) - I$. Denote by Cr the set of points for which Newton method is not defined, i.e. $Cr = \{z, |DT^k(z) - I| = 0\}$. Consider the set $P_1 = P \setminus (P \cap Cr)$. This is the set

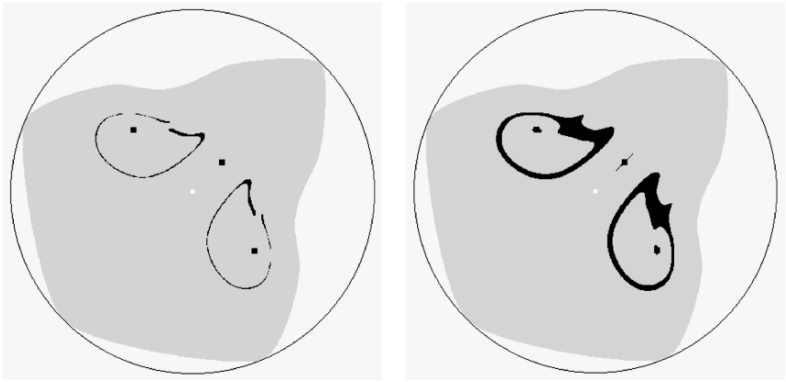

Fig. A.5. The sets P for $\varepsilon = 0.01228$ and $\varepsilon = 0.06$

of the first approximations to the roots of the equation $T^k(z) - z = 0$. As the map T specifies a two-degree polinomial, the equation has the power $2k$. Hence, it is requared to find $2k$ roots of the equation $F(z) = 0$. The results of numerical explorations show that not all points from the set P_1 are the initial approximation points for Newton's method. Assuming that a point $z_0 \in P_1$ is an initial approximation of a root of the given equation, we find its successive aproximations by Newton's method. It should be noted that even though the process converges, the inequality $KRL < 0.25$ from Theorem 25 may not hold for some $z_0 \in P_1$. In this case we take for x_0 the iteration z_l for which the inequality holds.

If Newton's process converges to a point z^* we determine its stability type calculating the eigenvalues of the matrix $DT^k(z^*) - I$. One need find only two points with different stability type which Newton's process converges to. Denote by z^*_{st} the stable point and z^*_{sd} the saddle one. Then their orbits may be considered as the first approximations to the k-periodic orbits. Actually,using this method we obtain an ε-trajectory with period k, where $\varepsilon = \rho(z^*_s, T^k(z^*_s))$ and $''s''$ denotes either $''st''$ or $''sd''$.

A.3.2 Refinement of Periodic Orbits

Proposition 188. [3] *1. The derivative of the map T is Lipshitz with constant $L = 2\lambda\mu$ in U.*

2. Providing that the conditions $\lambda < 1, \mu > 0$ are fulfilled the derivative of the map $F(z) = T^k(z) - z$ is Lipshitz with constant $L = 2d(\alpha + \beta)^k$ in U, where $\alpha = 1 - \lambda,\ \beta = \lambda\mu,\ d = 2\sqrt{2}r$.

Construct the periodic orbits *SdOrb* and *StOrb* starting from the points z^*_{sd}, z^*_{st} (the initial approximations are equal to z^1_0 and z^2_0 respectively). According to the above proposition the derivative of the map $F(z)$ is Lipshitz. Calcucate the values R_1, R_2, where $R_1 = ||DF(z^1_0)^{-1}F(z^1_0)||, R_2 = ||DF(z^2_0)^{-1}F(z^2_0)||$. For the points from the sets *SdOrb* and *StOrb* find the pair (saddle,sink) such that the distance between them (denoted by ρ) is minimal. Then the size of the vicinity where a root of the equation lies may be chosen as $\min\{R_1, R_2, \rho/2\}$. Hence, the points of the orbits of the first approximation are enclosed by nonoverlapping neighbourhoods $\{V_i\}$ and we can use Theorem 26 to construct the true orbits. The 7-periodic orbits of the map T were obtained for the following parameter values: $\lambda = 0.51260309232291;\ \mu = 4.11;\ h = 1/2000;\ \varepsilon = h$.

The set of the first approximations P_1 in a neighbourhood on of the non-diagonal fixed points is given in Table A.2. The points from P_1 (belonging to the orbits of different kinds) for which Newton's method converges are given in Table A.3. For the first point the constants from Theorem 25 are the following:

$$L = 2753.87180686379, \quad K = 1.06329193217488,$$

Table A.2.

The set of first approximation			
x	y	x	y
0.91519053028092	0.16117104015014	0.91954399154033	0.16291242465391
0.92999229856293	0.16813657816521	0.93434575982235	0.17074865492086
0.93956991333364	0.17423142392839	0.94305268234118	0.17684350068404
0.75759523269007	0.20818842175183	0.75672454043819	0.20905911400372
0.75585384818631	0.20992980625560	0.73321584963735	0.23866265056774
0.73147446513358	0.24127472732339	0.72973308062982	0.24388680407904
0.72799169612605	0.24649888083469	0.72625031162228	0.24911095759034
0.99007006394287	0.28655072442131	0.99007006394287	0.28742141667320
0.96656137314202	0.43805117624897	0.96569068089014	0.44066325300462
0.96307860413449	0.44762879101969	0.95698375837131	0.46678402056112
0.95611306611942	0.46939609731677	0.95524237386754	0.47287886632430
0.74192277215618	0.53121524720047	0.90474222325832	0.53208593945235
0.90474222325832	0.53295663170423	0.74366415665995	0.53382732395612
0.90387153100644	0.53382732395612	0.90387153100644	0.53469801620800
0.74540554116371	0.53643940071177	0.89516460848761	0.55472393800131
0.89516460848761	0.55559463025319	0.89429391623572	0.55733601475696
0.89429391623572	0.55820670700884	0.88819907047254	0.66007770047917
0.88732837822066	0.66094839273105	0.88645768596878	0.66181908498293
0.88732837822066	0.66181908498293	0.87426799444241	0.66617254624235
0.87513868669429	0.66617254624235	0.87600937894618	0.66617254624235

Table A.3.

The convergence points				
initial point		result		
x	y	x	y	type
0.91519053028	0.16117104015	0.912391624536	0.160105567817	saddle
0.89429391623	0.55820670700	0.894754262324	0.556339195966	stable

$$R = 0.00021927999662, \quad KRL = 0.642089036344767.$$

For the second point these constants are equal

$$L = 2753.87180686379, \quad K = 0.76224726788667,$$

$$R = 0.00026423675833, \quad KRL = 0.554667639692385.$$

So, R_1=0.00021927999662, R_2=0.00026423675833.

The approximate orbits constructed for the points from Table A.3 are shown in Table A.4. As seen from the data, these orbits are (p, ε)-trajectories with $p = 7$ and $\varepsilon = 10^{-8}$.

Table A.4.

Approximation of the saddle orbit		Approximation of the stable orbit	
x	y	x	y
0.9123916245362	0.1601055678173	0.8947542623246	0.5563391959663
0.7280018183558	0.2464380117305	0.9561129376275	0.4695532838862
0.7460716663694	0.5372912311996	0.9907531588342	0.3172621741925
0.8874029104849	0.6610044350345	0.9392371359164	0.1739336957911
0.9046037737272	0.5326807061340	0.7604877264424	0.2050113035449
0.9653506381715	0.4414347801262	0.7140289360308	0.4836671372821
0.9899825159836	0.2856238007974	0.8741531580855	0.6659284970523
0.9123916199167	0.1601055624441	0.8947542806894	0.5563391822603

Table A.5.

The saddle 7-orbit		The stable 7-orbit	
x	y	x	y
0.9123916150407	0.1601055603641	0.8741529679879	0.6659283848862
0.7280018132088	0.2464380194013	0.8947542480865	0.5563397417942
0.7460716722669	0.5372912400927	0.9561128010091	0.4695535736031
0.8874029121721	0.6610044334643	0.9907555556419	0.3172131322644
0.9046037758254	0.5326807028257	0.9392374323408	0.1739339535371
0.9653506398601	0.4414347751477	0.7604882250030	0.2050108805026
0.9899825157887	0.2856237952711	0.7140286530890	0.4836663837345

The points (0.887402910484926, 0.661004435034576) and (0.874153158085516, 0.665928497052353) are the most close with $\rho/2 \approx 0.00706$. In line with Theorem 26, the size of V_i is $\min\{2R_1, 2R_2, \rho/2\} = 0.00044, \varepsilon$ is 10^{-8} and

$$a = 2.10828189573076,\ L = 4.21359741887862,\ K = 3.19327339144196,$$
$$\sigma = 0.00010611199917,\ LK^2\left(\tfrac{a^p-1}{a-1}\right)^2\epsilon = 0.118610200921989.$$

Table A.5 shows the refined orbits.

The obtained orbits are depicted in Fig. A.6. The periodic orbits in a vicinity of the point O_3 are shown as well, being circle signs mark saddles and filled cirles mark sinks.

It should be noted that the results of the construction of the first approximation both using symbolic dynamics methods and the lattice method with the refinement by Newton's method are practically the same. The value of ϵ when constructing the set P is in the interval (0.0001,0.001). Newton's method for orbits converges for 4-5 iteration. The orbit is obtained with accuracy 10^{-9}.

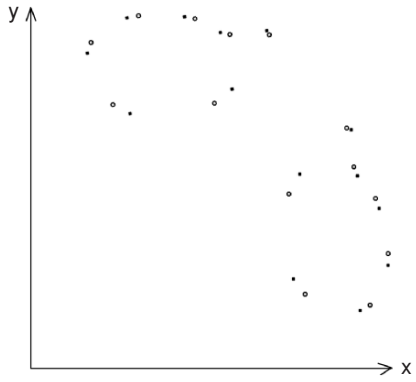

Fig. A.6. 7-periodic orbits in a vicinity of the invariant curve

References

1. N. Ampilova, A. Osipov, *Local bifurcations for Gardini map,* VINITI, 14.06.96, no. 1969-B96
2. N.B. Ampilova, Numerical investigation of invariant curves behaviour in the vicinity of a fixed point of the Gardini map, *Nonlinear dynamical systems,* v.1, Ed. G.Leonov, St. Petersburg, 1997, 5–13
3. N.B. Ampilova, Numerical methods of the construcrtion of periodic orbits near invariant curve for Hopf bifurcation, *Nonlinear dynamical systems*, v.2, Ed. G. Leonov, St. Petersburg, 2000, 71–80
4. V.I. Arnold, Loss of stability of oscillations close to resonant and versal deformation of equivariant vector fields, *Functional analysis and applications*, v.11, 1977, 1–10
5. D.G. Aronson, M.A. Chory, G.R. Hall and R.P. McGehee, Bifurcation from an invariant circle for two-parameter families of maps of the plane: a computer-assisted study, *Commun. Math. Phys.* 83, 3(1982), 303–354
6. L. Gardini, R. Abraham, R.J. Record, D Fournier-Prunaret, A double logistic map, Int. J. Bifurcation and Chaos, 1994, v.4, 145–176
7. D. Whitley, Discrete dynamical systems in dimensions one and two, *Bull. London Math. Soc.*, 15(1983), 177–217
8. J. Hale, H. Kocak, *Dynamics and Bifurcations*, Springer-Verlag, 1991

B

Implementation of the Symbolic Image

Danny Fundinger,
University of Stuttgart,
Institute of Parallel and Distributed Systems,
Universitätsstraße 38, 70569 Stuttgart, Germany,
research@danny.fundinger.de

The construction of the symbolic image is the basic task for investigations based on symbolic analysis. Once the system flow has been transformed into such a graph, all investigation tasks can be formulated as graph algorithms. Hence, an efficient implementation of this construction process is crucial for every investigation. In this chapter, we propose algorithms and adequate data structures which are appropriate to achieve this task. Additionally, we introduce some basic investigation methods on the graph in order to apply the implementation in practice. A theoretical analysis regarding the performance and accuracy of the computations is given. Afterwards, we focus on several important aspects of a practical application. Several extensions and tunings of the original concepts are proposed which extend the field of application for the method. We discuss these techniques and, if necessary, also mention some aspects of implementation and useful heuristics for an efficient usage. Numerical computations are performed for several dynamical systems in order to verify the proposed implementation. We study some reasonable parameter settings and the steps to be taken for the acquisition of the data. While doing so, the reader will be introduced to possible fields of application for symbolic analysis.

Acknowledgements

The author would like to thank V. Avrutin for discussions and for contributing some numerical computations to this work (Fig. B.2). The author also thanks G. Söderbacka for discussions about the Coupled Logistic Map.

B.1 Implementation Details

From the viewpoint of an implementation by a computer program, the principle scheme of every investigation can be considered as an iterative process which will be repeated for increasing levels of phase space discretization. At each level the calculation involves three main steps which have to be performed several times:

1. Subdivision of selected parts of the phase space into smaller parts.
2. Construction of the symbolic image for the current discretization of the phase space.
3. Application of an investigation method on the symbolic image graph. As a result, parts of the state space get selected for further subdivision and a more precise investigation.

These steps will be repeated until a termination criterion is fulfilled. This condition depends on the desired accuracy as well as on the existing computation power, see Sect. B.1.3.

In this section we describe the implementation of this basic framework and discuss those aspects which have to be taken into consideration for an efficient implementation. The basic framework as proposed here was implemented and tested within the Ant-project [3], a larger, non-commercial software package for the investigation of dynamical systems. The software is available for download, see [1].

B.1.1 Box and Cell Objects

In order to build a symbolic image for a domain $M \subset \mathbb{R}^d$ of the phase space, a finite covering $C = \{M(1), \cdots, M(n)\}$ has to be defined. In contrast to the theoretical approach, it is usually not possible to cover the complete domain $\mathcal{M}$ of the function f. Instead, in a practical approach we choose an area of investigation $M \subset \mathcal{M}$ in such way that we assume all important dynamics happen inside this area. Note, however, that usually only those objects can be detected by investigations of symbolic images which are completed covered by M. Generally, there are no restrictions concerning the geometry of M and of the sets $M(i) \in C$, except that they have to be closed and compact. The investigated domain M could be any confined part of the phase space and has to be provided by the user. For the simplicity of the implementation we assume here that it is an d-dimensional rectangular region:

$$M = \left[M_1^{\min}, M_1^{\max}\right] \times \cdots \times \left[M_n^{\min}, M_n^{\max}\right]. \tag{B.1}$$

Then we can subdivide the area M into *uniform grid boxes*. In order to do this, the user has to define for each state space coordinate k ($k = 1, \ldots, d$) the numbers $i_k^{\max}$ of subdivisions for the domain M. Then M can be subdivided into

$$m = \prod_{k=1}^{d} i_k^{\max} \tag{B.2}$$

d-dimensional rectangular boxes. The length of the edge k is given for each box by

$$d_k(M(i)) = \frac{1}{i_k^{\max}} \left(M_k^{\max} - M_k^{\min} \right). \tag{B.3}$$

Every box must hold the information about its position in the d-dimensional state space. In context of an efficient implementation, the positions of boxes are represented as d-dimensional *multi-indices* $\mathrm{i} \in \mathbb{N}^d$,

$$\begin{aligned} &\mathrm{i} = (i_1, \ldots, i_d) \in \mathbb{N}^d \\ &\text{with} \quad i_k \in [1, \ldots, i_k^{\max}], \quad \forall k = 1, \ldots, d, \end{aligned} \tag{B.4}$$

so that for every box $M(\mathrm{i}) \in C$ exists a unique multi-index I defining its position in M.

This representation was chosen because it allows a fast and easy mapping from $\mathbf{x} \in M(\mathrm{i})$ to i and vice versa. Furthermore, the mapping range within the domain of usual integer values is much larger if multi-indices are used instead of one-dimensional indices. If N_{int} is defined as the maximal integer value of a computer system and one would only use one-dimensional indices to identify the boxes $M(i)$ then each $i \in \{1, \ldots, N_{\mathrm{int}}\}$. An area of investigation M could only be subdivided in $m = N_{\mathrm{int}}$ boxes because no more values are available for the description of all possible positions. Note that there must be an index for every position i, no matter if $M(i)$ exists or not. This is a crucial restriction for higher-dimensional systems. If multi-indices are used instead, an d-dimensional domain M can be subdivided in $m = (N_{\mathrm{int}})^d$ boxes which means we have an exponential growth for the number of possible box positions.

After the construction of the covering C is completed, an approximation of the symbolic image based on C can be constructed. It represents a graph G, whereby the vertices of G correspond to the boxes $M(\mathrm{i})$ of C. In the following, we denote the vertices of G as *cells* c_I. Each of these cells c_I is uniquely connected with a box $M(\mathrm{i})$. This correspondence represents the link between the domain M and the symbolic image G. The edges of the graph G are defined by *adjacency lists*. To each cell belongs such a list with its target cells. Note that we do not use an *adjacency matrix* for the representation of the edges. Reason for this is that the symbolic image graph is considered to be huge but sparse. Hence, an adjacency matrix would require by far more memory resources than the lists.

B.1.2 Construction of the Symbolic Image

The construction of a symbolic image based on numerical calculations is always only an estimation of the "real" symbolic image G. Besides the usual

numerical errors which occur by the computation of a mapping $f(\mathbf{x})$ for $\mathbf{x} \in M$, another reason for this is the fact that the construction of the image

$$T(\mathrm{i}) = f(M(\mathrm{i})) = \{\mathbf{y} \mid \mathbf{y} = f(\mathbf{x}), \mathbf{x} \in M(\mathrm{i})\} \subset \mathbb{R}^d \tag{B.5}$$

for a box $M(\mathrm{i})$ would involve the calculation of $f(\mathbf{x})$ for every $\mathbf{x} \in M(\mathrm{i})$. This is, of course, beyond the limits of every finite numerical computation.

In our implementation, the image $T(\mathrm{i})$ is approximated by a finite set of points. This technique was also used for the implementation of similar numerical methods [7, 12], and has proved to be an efficient and reliable approach in practice. From each box $M(\mathrm{i})$ a representative set of k points is selected,

$$S(\mathrm{i}) = \{\mathbf{x}_j \mid \mathbf{x}_j \in M(\mathrm{i}), \quad j = 1 \ldots k\} \tag{B.6}$$

the so-called *scan points* of the box $M(\mathrm{i})$. Then the approximation $\tilde{T}(\mathrm{i})$ of the region $T(\mathrm{i})$ in the state space is calculated by

$$\tilde{T}(\mathrm{i}) = f(S(\mathrm{i})) = \{\mathbf{y}_j \mid \mathbf{y}_j = f(\mathbf{x}_j), \mathbf{x}_j \in S(\mathrm{i})\} \tag{B.7}$$

As one can see, the continuous region $T(\mathrm{i})$ will be approximated by the discrete set $\tilde{T}(\mathrm{i}) \subset T(\mathrm{i})$ consisting of k points. The number k of scan points for the boxes as well as the positions of these points within the boxes are parameters of the described method, which must be set by the user. A general strategy how the scan points should be placed within the box $M(\mathrm{i})$ is that they are either uniformly distributed within $M(\mathrm{i})$ or that they are put into the neighborhood of the boundaries.

Besides the calculation of scan points, a mapping

$$p : M \mapsto \mathbb{N}^d, \quad \forall \mathbf{x} \in M(\mathrm{i}) \;\Rightarrow\; p(\mathbf{x}) = \mathrm{i} \tag{B.8}$$

of a point $\mathbf{x} \in M(\mathrm{i})$ onto a box index i is required for further computations. Additionally, we need its inverse mapping

$$p^{-1} : \mathbb{N}^d \mapsto M, \quad \forall \mathrm{i} : \quad p^{-1}(\mathrm{i}) = \mathbf{x} \;\Rightarrow\; \mathbf{x} \in M(\mathrm{i}) \tag{B.9}$$

which defines for every $M(\mathrm{i})$ the spatial coordinates of a point within this box. Note that $p^{-1}(\mathrm{i})$ is only defined if $M(\mathrm{i})$ exists for i.

Due to the fact that all uniform grid boxes have the same size, the mapping $p : M \mapsto \mathbb{N}^d$ can be simply defined as

$$p(\mathbf{x}) = \mathrm{i} = (i_1, \ldots, i_d) \tag{B.10}$$

$$\text{with } i_k = \left\lfloor \frac{\mathbf{x}_k - M_k^{\min}}{i_k^{\max}} \right\rfloor + 1, \quad k = 1, \ldots, d$$

The inverse mapping can be described in a similar way. Note, however, that the inverse mapping is not unique and, in practice, requires the definition of

an arbitrary reference point within the box $M(\mathrm{i})$. If using, for instance, the minimal point of each box, one can get

$$\begin{aligned} &p^{-1}(I) = \mathbf{x} = (x_1, \ldots, x_d)^T \\ &\text{with } x_k = M_k^{\min} + (i_k - 1) \cdot d_k(M(\mathrm{i})),\ k = 1, \ldots, d \end{aligned} \tag{B.11}$$

After the functions p and p^{-1} have been defined, the approximation $\tilde{C}(\mathrm{i})$,

$$\tilde{C}(\mathrm{i}) = \left\{ M(\mathrm{i}') \mid M(\mathrm{i}') \cap \tilde{T}(\mathrm{i}) \neq \emptyset \right\}, \tag{B.12}$$

of the covering $C(\mathrm{i})$,

$$C(\mathrm{i}) = \left\{ M(\mathrm{i}') \mid M(\mathrm{i}') \cap T(\mathrm{i}) \neq \emptyset \right\}, \tag{B.13}$$

can be computed. Obviously, we have the relation $\tilde{C}(\mathrm{i}) \subseteq C(\mathrm{i})$.

Proceeding this task, the following steps have to be performed for each box $M(\mathrm{i})$ in the covering C :

1. The set of scan points $S(\mathrm{i})$ is calculated using a set of k globally defined relative coordinates

   $$S = \left\{ \xi_j \,|\xi_j = (\xi_{j,1}, \ldots, \xi_{j,d})^T, \xi_{j,i} \in [0,1], i = 1..d, j = 1..k \right\} \tag{B.14}$$

   with respect to the reference point $\mathbf{x}_0 = p^{-1}(\mathrm{i})$:

   $$S(\mathrm{i}) = \{ \mathbf{x}_j \,|x_{j,i} = x_{0,i} + \xi_{j,i} \cdot d_i(M(\mathrm{i})), i = 1..d,\ \xi_j \in S, j = 1..k \} \tag{B.15}$$

   This is necessary for scaling the relative coordinates ξ_j, which are defined within the hypercube $[0,1]^d$, onto the area $M(I)$.
2. For every point $\mathbf{x}_j \in S(\mathrm{i})$ the target point $\mathbf{y}_j \in \tilde{T}(\mathrm{i})$ will be calculated. Dealing with dynamical systems discrete in time, i.e. $\mathbf{x}_{k+1} = f(\mathbf{x}_k)$, the target point $\mathbf{y}_j$ can be found by a simple one step iteration of the point $\mathbf{x}_j$:

   $$\mathbf{y}_j = f(\mathbf{x}_j) \tag{B.16}$$

   Note that also the n-th iterated function f^n can be used in Eq. B.16 instead of f. This is necessary if we want to apply symbolic images to dynamical systems continuous in time, see Sect. B.5.1, or if we want to work with higher iterated functions, see Sect. B.6 for a more detailed discussion.
3. For each target point $\mathbf{y}_j \in \tilde{T}(\mathrm{i})$ the corresponding box object $M(\mathrm{i}')$ with $\mathbf{y}_j \in M(\mathrm{i}')$ must be found.
   The index i' of this box is given by

   $$\mathrm{i}' = p(\mathbf{y}_j) \tag{B.17}$$

   It is important to check, whether the conditions

$$1 \leq i'_k \leq i_k^{\max} \quad \forall k = 1, \ldots, d \tag{B.18}$$

hold for the components of the multi-index i'. If not, the index i' exceeds the dimension range and there is no box defined for this index.

4. Within the implementation context, a memory access function

$$\mathbf{g} : \mathbb{N}^d \mapsto M, \ \exists M(\mathrm{i}) \in C \ \Rightarrow \ \mathbf{g}(\mathrm{i}) = M(\mathrm{i}) \tag{B.19}$$

is required in order to access a box object $M(\mathrm{i})$ for an index i. In our approach, a hash map H is used which contains a key i iff there exists a corresponding $M(\mathrm{i})$. Hence, no memory space is wasted for indices without a corresponding box object. Note that a fast and proper implementation of H requires the definition of a *strict weak order* relation $\prec$ for the box indices i of a covering C. This can be achieved by applying an iterative comparison of the components i_k $(k = 1, \ldots, d)$ of an index I, starting with the largest "digit" i_d:

$$\begin{aligned} &\mathrm{i} \prec \mathrm{i}' \quad \text{iff} \quad \exists k = 1, \ldots, d \\ &\text{with} \quad i_k < i'_k \quad \text{and} \quad i_j = i'_j \quad \forall j > k. \end{aligned} \tag{B.20}$$

5. If $M(\mathrm{i}')$ has been located, a reference to it will be added to the list of $\tilde{C}(\mathrm{i})$. When the location of the target boxes $M(\mathrm{i}')$ for all scan points $\mathbf{x}_j \in S(\mathrm{i})$ is completed, the list of $\tilde{C}(\mathrm{i})$ is an estimation of the covering $C(\mathrm{i})$ for the box object $M(\mathrm{i})$.

After the described steps were performed for all boxes of the state space discretization, an approximation G of the symbolic image has been constructed. The vertices of the graph are the cells c_I corresponding to the boxes $M(\mathrm{i})$. For each c_I the adjacency list of target cells is given by the cells corresponding to the boxes of the covering $\tilde{C}(\mathrm{i})$.

B.1.3 Subdivision Process

In the previous section, the construction of a symbolic image G was described. It was already mentioned that the precision of the state space discretization for such a symbolic image is increased by an iterative process. To describe this process, we introduce an index s which indicates the level of state space discretization, $s = 0, 1, \ldots$, or, in other words, the subdivision depth of a symbolic image. In the following, the notation for the symbolic image G is extended to G^s. The notation C^s, I^s and so on is introduced in the same way.

In order to get the new graph G^{s+1} for a G^s, a new covering C^{s+1} has to be calculated. This covering depends on a selection of cells $SV(G^s) \subseteq V(G^s)$ chosen by the application of an investigation method to the graph G^s. The covering C^{s+1} usually covers only parts of the area covered by C^s. Let c_{i^s} be the cell in G^s which matches to the box $M(\mathrm{i}^s)$. Then the new area of

investigation is given by the joint of all boxes which belong to a selection of cells $SV(G^s)$:

$$M^{s+1} = \bigcup_{c_{\mathrm{i}^s} \in SV(G^s)} M(\mathrm{i}^s). \tag{B.21}$$

Each of these boxes will be divided into m sub-boxes $M(\mathrm{i}^{s+1})$, see Eq. B.2, which build together the new covering C^{s+1}. For every $\mathrm{i}^s = (i_1, \ldots, i_d)$ the m new indices i^{s+1} are defined as follows:

$$\begin{aligned} &\mathrm{i}^{s+1} = \left(j_1 + (i_1 - 1) \cdot i_1^{\max},\ \ldots\ ,\ \ j_d + (i_d - 1) \cdot i_d^{\max}\right) \\ &\text{with} \quad j_k = 1, \ldots, i_k^{\max} \quad \forall k = 1, \ldots, d \end{aligned} \tag{B.22}$$

After the subdivision, the graph G^{s+1} is constructed for the covering C^{s+1} as described in Sect. B.1.2, and the whole calculation process is repeated.

It is a distinctive feature of the methods of symbolic analysis that only the covering of the current subdivision step is subject of investigation. Hence, after parts of a covering C^s are selected and subdivided into a more precise covering C^{s+1} then C^s can be deleted. This is essential for an efficient usage of the memory resources. It is furthermore assumed that each covering C^s, except the initial covering C^0, does only cover parts of the area of investigation M.

B.2 Basic Investigations on the Graph

In this section we discuss some basic investigation techniques that can be applied to the symbolic image graph. Note that we use variations of some standard graph algorithms. A discussion of the original algorithms is out of scope of this work, therefore we refer to [1, 4].

B.2.1 Localization of the Chain Recurrent Set

The most important kind of investigation technique on the graph is the localization of the recurrent cells. Applying this technique, we can determine a neighborhood of the chain recurrent set Q. Theorem 16 in Chapter 6 states that the chain recurrent set can be approximated as precisely as one likes by the methods of symbolic analysis. The symbolic image must be constructed and subdivided for several times. The cells which have to be selected for subdivision are those which are recurrent. Hence, we propose now an algorithm for the localization of the recurrent cells in a symbolic image. Note that almost all other investigation methods of symbolic analysis also require the detection of the recurrent cells. Therefore, this technique is considered as a general first computation step of all investigations on a symbolic image graph.

An efficient approach to detect the recurrent cells is the variation of Tarjan's algorithm for the calculation of strongly connected components in directed graphs [22]. This algorithm locates the strongly connected components of a directed graph G by a *depth-first search*. Two vertices a and b of G are said to be strongly connected ($a \sim b$) if there exists a path from a to b and from b to a. Furthermore, the relation $a \sim a$ (reflexivity) always holds by definition. It can easily be proved that $\sim$ is an equivalence relation and that therefore G will be partitioned by the relation $\sim$ into equivalence classes, the strongly connected components. Although recurrent cells of G and strongly connected vertices are not the same, they are closely related to each other. If

$$\gamma_a = \{b \mid a \sim b\} \tag{B.23}$$

is a strongly connected component for which there is a path from a to each b and vice versa with $a \neq b$ then, for a as well as b, exists a periodic path. It follows that, if $|\gamma_a| > 1$, then for all cells $c \in \gamma_a$ exists a periodic path and therefore all these cells are recurrent. The special case to look at is $|\gamma_a| = 1$. Due to reflexivity, if there is only one component in the set it could mean that this cell is either non-recurrent or, if there is an edge $a \rightarrow a$, its least period size is 1.

So, for the localization of recurrent cells, Tarjan's algorithm needs a minor extension. What has to be done in addition is to perform a test for each set γ_a if $|\gamma_a| = 1$ holds. In this case, it has to be checked for the single cell of this set whether it is one-periodic (or recurrent), which means one of its target cells is itself, or not. If the cell is not one-periodic, it is non-periodic (or non-recurrent). All cells belonging to a set γ_a with $|\gamma_a| > 1$ are periodic, i.e. recurrent. All recurrent cells that belong to the same set γ_a can be considered as a set of equivalent recurrent cells which we denote in the following by H_k. Furthermore, we define the union of these sets by $\zeta = \{H_k\}$.

B.2.2 Localization of Periodic Points

A related investigation is the localization of p-periodic points $P(p) = \{\mathbf{x}| f^p(\mathbf{x}) = \mathbf{x}, \mathbf{x} \in M\}$ for a given value p. Theorem 23 states that the set of p-periodic points can be approximated as precisely as one likes by the methods of symbolic analysis. The symbolic image must be constructed and subdivided for several times. The cells which have to be selected for subdivision are those which are p-periodic. Hence, we propose now an algorithm for the localization of the periodic cells in a symbolic image.

For a practical application of Theorem 23, we have to consider that there might be more than one admissible path to which a cell c_i belongs to, especially in case of a coarse phase space discretization. Indeed, the number of admissible paths to which a cell belongs can even be infinite. In that case, it is impossible to explicitly compute each periodic path to which the cell belongs. On the other hand, if each cell of a symbolic image represents exactly

one periodic point in the phase space then this cell c_p belongs only to one p-periodic path $\{\dots, c_{i_0}, \dots\}$ with $c_{i_0} = c_p$. Although such a precise covering can not be achieved by numerical computation, a reasonably fine phase space discretization is usually sufficient to get a unique path for a cell which belongs to a covering of a periodic point. Considering these facts, the p-periodic points can be located by selecting all cells for subdivision which have a *shortest periodic path* for a period $p' \leq p$. Obviously, such a selection contains all cells which belong to a p-periodic path. After several subdivisions, we check that there exists a unique periodic path for each cell of the symbolic image. In case this can not be achieved, a higher precision of the symbolic image is required, i.e. more subdivisions must be applied.

Consequently, an algorithm is needed which is able to find the shortest periodic path $c_i \to \cdots \to c_i$ for every recurrent cell c_i on the symbolic image graph. Furthermore, the length of such a path must be detected. Note that Tarjan's algorithm is not capable to solve this task. Instead, we introduce a different algorithm which is based on the idea of Dijkstra's algorithm for calculation of shortest paths in directed graphs [8]. It belongs to the class of so-called *greedy algorithms* and performs a *breadth-first search*.

The Dijkstra algorithm does not only find the shortest paths from each cell c_i to all other cells of the graph, but also locates at the k-th step first the path $c_i \to \cdots \to c_u$ so that the following equation is fulfilled:

$$d(c_i, c_u) = \min\{d(c_i, c_v) \mid c_v \in V(G) \wedge (c_i \to \cdots \to c_v) \notin D_{k-1}\}, \quad \text{(B.24)}$$

where $d(c_i, c_u)$ is defined as the length n of the shortest path between c_i and c_u, and D_{k-1} is the set of all shortest paths which have already been detected in the previous steps. Then the shortest periodic path of a cell c_i can be found by checking for the first detected shortest path $c_i \to \cdots \to c_u$ whether the edge $c_u \to c_i$ exists. If so, the algorithm can be stopped because the path $c_i \to \cdots \to c_u \to c_i$ is the shortest periodic path for the cell c_i and the length of this path is the period of c_i. If not, then the next shortest path has to be detected and checked for the same condition until a periodic path has been found or until all shortest paths have been visited.

There are several improvements to speed up Dijkstra's algorithm within our context. First of all, the original Dijkstra algorithm is developed for weighted graphs while the edges of G are unweighted. This means that the edge weight $\gamma(c_i \to c_j)$ is 1 for all edges of G. Therefore, the outer edge of visited but not yet examined cells can be implemented as a queue. Every cell which is visited first time and becomes a part of the outer edge will be pushed into the queue, while the next cell which will be examined can be popped out of the queue. This works fine because our edges are unweighted and so the distance between c_i and the first element in the queue is always the minimum distance between c_i and every other element in the queue.

Next it should be considered that all periodic cells of G have to be inspected. So in worst case, the modified Dijkstra algorithm must be started once for each cell $c_i \in V(G)$. In order to spare out some of the cells, we can

first run the Tarjan algorithm to detect the recurrent cells and the sets ζ of equivalent recurrent cells. The Dijsktra algorithm must then only be started for the recurrent cells $c_i \in RV(G)$. Furthermore, it is sufficient to check for each of these cells only the paths to equivalent recurrent cells, i.e. those cells which belong to the same set $H_k \in \zeta$. Cells which do not belong to the same set can not belong to the same shortest periodic path.

Despite all improvements, the modified Dijkstra's algorithm can not compete with the performance of the aforementioned Tarjan's algorithm. So it should only be chosen by the user if the additional information about the periodic paths and/or the least period sizes are really required for the calculation.

B.3 Performance Analysis

The performance of symbolic image construction as described above is analysed by studying the *worst-case scenario* for the time complexity. We use the standard *O-notation*. In the following, n_s denotes the number of cells in the symbolic image G^s.

Proposition 189. [2] *The construction of the symbolic image G^s with respect to the covering C^s is in $O(n_s \log(n_s))$.*

In order to construct G^s, we consider a function *getBoxMapping*$(M(\mathrm{i}))$ which is called for every box $M(\mathrm{i}) \in C^s$. This function calculates an estimation $\tilde{C}(\mathrm{i})$ for $C(\mathrm{i})$ by first locating all indices i' with $M(\mathrm{i}') \in \tilde{C}(\mathrm{i})$ and afterwards accessing these boxes by calling the function $\mathbf{g}(\mathrm{i}')$, see Eq. B.19. Each call of *getBoxMapping*$(M(\mathrm{i}))$ is in $O(\log(n_s))$. Hereby, the computation time depends on a constant c which is governed by the number of scan points, $|S|$, and a number m_f so that $c = m_f\,|S|$. Note that m_f describes the number of function iterates, see Sects. B.5.1 and B.6. The size of the constant c is significant for the practical computation.

These results are closely related to the proposed method for the approximation of the covering $C(I)$. The number of edges for a cell is limited by the scan points per box, and in our case this is a constant. If another approach is chosen for the approximation of the covering like, e.g. interval arithmetic [11] or the calculation of the Lipschitz constant [15], the number of edges per cell is not longer bounded by a constant. For the performance analysis this means that the time complexity must possibly be multiplied by n_s.

Proposition 190. [2] *The construction process and investigation of a symbolic image for a subdivision phase s can be done in time $O(n_s \cdot \log(n_s))$ if only recurrents cells are located using Tarjan's algorithm, and in time $O(n_s^2)$ if the least period size and the shortest periodic path for each cell should also be calculated.*

The time required for the computation of recurrent cells is within $O(n_s \cdot \log(n_s))$, and therefore almost ideal from the theoretical point of view, especially for large n_s. Hereby, the construction of the symbolic image requires the main computational effort. The effort for the subdivision of cells as well as the localization of recurrent cells can be neglected. The time complexity changes in case the least period sizes and shortest periodic paths are computed by application of the algorithm proposed in Sect. B.2.2. Then the investigation of the graph can require by far more computational effort than the graph construction.

Performance analysis shows that the computation time of the algorithms is no major obstacle for the construction of the symbolic image. Instead, the crucial factor is the size of the input value n_s, i.e. the memory resources required for a computation. Note that n_s could grow almost exponential during the subdivision process. The size and growth rate of n_s depend hereby not only on the investigation task, i.e. the dimension of those objects which are the subjects of investigation, but also on the specific properties of the focused dynamical system. Practical application has shown that a high growth rate of n_s is a limitation for many computations. Hence, it should be the main concern to keep the number of cells n_s low and avoid an high growth rate during subdivision. Often this can be achieved by appropriate parameter settings or tunings of the method, see Section B.6.

B.4 Accuracy of the Computations

Let us next consider the accuracy of the numerical calculation. One should recall that we do not calculate specific points in the domain space but boxes $M(\mathrm{i})$ with some extent. These boxes are always only an outer covering of a solution. In our implementation, a box $M(\mathrm{i})$ is defined as a uniform grid box. The size of such a grid box defines the accuracy ϵ of the calculation. Let us denote by d_k the edge length of a grid box $M(\mathrm{i})$ on the dimension axis k, and by L^s the union of boxes which correspond to the selected cells $SV(G^s)$ in the symbolic image G^s constructed after the s-th subdivision. Then these boxes in L^s are neighborhoods (or an outer covering) of a solution S. The basic principle of symbolic analysis is that the sequence of embedded neighborhoods $L^0 \supset L^1 \supset \cdots \supset L^m$ gets for every subdivision step $s = 0, \ldots, m$ closer to S in the way that, if the largest edge length tends to zero as s becomes infinite, then,

$$\lim_{s \to \infty} L^s = \bigcap_s L^s = S. \tag{B.25}$$

See also Theorem 4 in Chapter 3 and Theorem 16 in Chapter 6 as examples of this principle. Unfortunately, for practical numerical calculations there is a minimal edge length which limits the accuracy. Reason for this is that the n-dimensional phase space covered by M, see Eq. B.1, gets divided into regions

which are identified by multi-indices $\mathrm{i} \in N^n$, Eq. B.4. As mentioned above, a value i_k of the k-th component of the multi-index i is represented by an integer value, and for every computation machine there exists a constant N_{int} giving the largest number which can be represented as an integer value. Consequently, we have the limitation $i_k^{\max} \leq N_{\mathrm{int}}$. Therefore, every edge length d_k is limited to

$$d_k^{\min} = \frac{M_k^{\max} - M_k^{\min}}{N_{\mathrm{int}}} \tag{B.26}$$

which means that the minimal error ϵ_k can only shrink down to $\epsilon_k \geq d_k^{\min}$.

Note that this limit is not specific for the presented method but only for the implementation presented in this work. Furthermore, it is possible to extend the limit to any size by taking a different representation of a number i_k, though this implies a higher memory consumption.

B.5 Extensions for the Graph Construction

We consider two important extensions of the proposed implementation. One is the integration of dynamical systems continuous in time, the other a technique for the better approximation of the image of a box. Both of these extensions aim to improve the construction of the symbolic image graph and extend the possible field of application for the methods of symbolic analysis.

B.5.1 Dynamical Systems Continuous in Time

Only dynamical systems discrete in time have been discussed so far. The symbolic image for such a system

$$\mathbf{x}_{k+1} = f(\mathbf{x}_k),\ x_k \in M$$

can be constructed by performing one iteration which means simply applying the system function $f(\mathbf{x})$ on the points $\mathbf{x} \in M(\mathrm{i})$ lying in a box $M(\mathrm{i})$ of a certain covering, see Eq. B.16. If we are dealing now with systems continuous in time given by an ODE, i.e. $\dot{\mathbf{x}} = \mathbf{F}(t, \mathbf{x})$, $t \in \mathbb{R}$, some kind of mapping is required which transforms an orbit continuous in time into one discrete in time. As already mentioned in Chapter 1, a shift operator along trajectories is needed. Such a shift operator $\phi(t, t_0, \mathbf{x}_0)$ is considered to be the solution of the vector field $\mathbf{F}$ with an initial condition $\phi(t_0, t_0, \mathbf{x}_0) = \mathbf{x}_0$.

In our implementation, we use a stroboscopic mapping with a fixed discretization time t. This approach is applicable if the underlying differential equation is autonomous. Such a shift operator has the form $f(\mathbf{x}) = \phi(t, \mathbf{x})$ with $\phi(0, \mathbf{x}) = \mathbf{x}$. It can be calculated by solving the equation

$$\dot{\mathbf{x}}(t) = \mathbf{F}(\mathbf{x}(t)) \tag{B.27}$$

for the time t and initial conditions $\mathbf{x}(0) = \mathbf{x}$. We assume a fixed $t > 0$. In that case, $\phi(t, \mathbf{x})$ is also called a *time-t map*. Such a time-t map is a restriction of ϕ to $M \times tZ$ and, hence, a discretization of the dynamical system continuous in time. Note that similar approaches for a discretization were also proposed in [14, 20].

Consider now that in the context of a computer implementation it is suitable to use a small integration step size Δt for the applied integration method in order to minimize numerical errors. Hence, we do not calculate $\phi(t, \mathbf{x})$ explicitly. Instead, we use an integration step size $\Delta t = t/n$ with $n \in N$ and iterate ϕ for n times so that

$$\phi(t, \mathbf{x}) = \phi(\Delta t \cdot n, \mathbf{x}) = \phi^n(\Delta t, \mathbf{x}).$$

This approach allows us the numerical computation of time-t maps for any precision, independently of the chosen discretization time t. In the following, we use the notation $f(\mathbf{x}) = \phi(\Delta t, \mathbf{x})$ so that the time-t map for a $t = \Delta t \cdot n$ is given by $f^n(\mathbf{x})$. Hence, the symbolic image is constructed assuming $f^n(\mathbf{x})$ as the system function instead of $f(\mathbf{x})$, see also the comments to Eq. B.16.

B.5.2 Error Tolerance for Box Images

As already stated, the construction of symbolic images requires the approximation $\tilde{C}(\mathrm{i})$ of the covering $C(\mathrm{i})$, see Eqs. B.12 and B.13. Note that for our proposed implementation there is $\tilde{C}(\mathrm{i}) \subseteq C(\mathrm{i})$, and so some boxes may get lost. This behavior can be reduced by usage of a large number of scan points for each box. A disadvantage of this approach is that the computation time may become inappropriately large. As another solution of the problem one can extend the covering $\tilde{C}(\mathrm{i})$ by boxes which correspond to boxes in its neighborhood. We define a small constant ϵ and introduce the extended covering

$$C^{\mathrm{ext}}(\mathrm{i}) = \big\{ M(\mathrm{i}') \mid \exists M(J) \in \tilde{C}(\mathrm{i}), \exists \mathbf{x} \in M(J), \exists \mathbf{y} \in M(\mathrm{i}'), \rho(\mathbf{x}, \mathbf{y}) \leq \epsilon \big\}. \tag{B.28}$$

Note that a suitable setting of the constant ϵ depends on the edge length $d_k(M(\mathrm{i}))$ of the boxes, Eq. B.3, and hence on the subdivision level. In our implementation, the user can define a parameter e, which is in the following denoted as the error tolerance, so that

$$\epsilon_k = e \cdot d_k \tag{B.29}$$

for the k-th phase space component. The condition $|x_k - y_k| \leq \epsilon_k$ is used instead of $\rho(\mathbf{x}, \mathbf{y}) \leq \epsilon$ in Eq. B.28. Note that d_k is the generalized edge length of the boxes in a covering C.

In practice, this parameter was used to detect p-periodic trajectories if they can not be found otherwise, whereby a setting of $e = 0.1$ proved to be sufficient in our simulations. One should keep in mind that the use of this

parameter usually increases the size of the symbolic image and, therefore, it should only be applied if necessary. Furthermore, it is often a good alternative to increase the number of scan points $S(\mathrm{i})$ for a more precise calculation instead of applying error tolerance. Some of the scan points should then be placed close to the corners of the boxes.

Note that this approach was motivated by the technique described in Junge [15]. Actually, if ϵ is calculated by Lipschitz constants as proposed by Junge, it could be guaranteed that $C(\mathrm{i}) \subseteq C^{\mathrm{ext}}(\mathrm{i})$.

B.6 Tunings for the Graph Investigation

Performance analysis has shown that the computation time of the algorithms is no major obstacle for the construction of the symbolic image. Assuming n_s is the number of cells belonging to a symbolic image G^s, i.e. $n_s = |V(G^s)|$, all computations can be performed in $O(n_s \cdot \log(n_s))$, see Prop. 190. Instead, the crucial factor is the size of the input value n_s or, in other words, the memory resources required for a computation. Note that n_s could grow almost exponential for $s \to \infty$, i.e. during the subdivision process. Ideally, this growth rate should only depend on the investigation task or, more precisely, the dimension of those objects which are the subjects of investigation. However, due to the complexity of the underlying dynamics, this is often not the case. Instead, we observed that in many computations much more cells are selected for subdivision than necessary. The major problem we come across is that not only those cells are selected which correspond to boxes containing parts of the solution, but also several more cells which correspond to boxes in the neighborhood of the solution. Reason for this is a too coarse discretization of the phase space. In the following, we will refer to this phenomenon as *clustering*. Due to clustering, the growth rate of the number of cells in a symbolic image increases during the subdivision process, and the accuracy of the computation shrinks. Moreover, the analysis of computed data is more difficult.

Taking the theoretical point of view, the selection of too many cells for subdivision does not matter. By successive application of the subdivision process the discretization of the phase space gets finer. Eventually, those boxes which do not contain a solution will be deleted and the solution is detected as precisely as one likes. However, taking the practical point of view, one has to deal with limited resources. That means that the number of applicable subdivisions is limited by the memory space of the computation machine which only allows the storage of a symbolic image graph of a limited size. Therefore, it is our strong concern to avoid clustering, i.e. the selection of cells for subdivision which do not contain a solution. This aim can only be achieved by a change of paradigm. The target is not anymore the rigorous construction of the symbolic image graph for a phase space discretization. We are not interested in providing all existing edges between the cells as requested in the theoretical approach, but rather more only those edges which are necessary

for the detection of the solution. By doing so, we are also aware of the fact that some important information might get lost. However, empirical studies have shown that numerical investigations are mostly limited by performance resources instead of an insufficient approximation of the symbolic image. A significant reason for this is that the method is typically quite robust.

B.6.1 Use of Higher Iterated Functions

When dealing with dynamical systems discrete in time $\mathbf{x}_{n+1} = f(\mathbf{x}_n)$, the points $\mathbf{y} \in \bar{T}(\mathrm{i})$, which represent the images of $\mathbf{x}$, are calculated as direct successors of the scan points: $\mathbf{y} = f(\mathbf{x})$. However, in some cases it is more suitable to use an iterated function of f and calculate the image points by

$$\mathbf{y} = f^n(\mathbf{x}), \quad n > 1 \tag{B.30}$$

In other words, the symbolic image is not constructed for the function f but for the n-th iterated function f^n. In the following, we will denote a symbolic image constructed for f by G_f and for f^n by $G_{f^{[n]}}$.

Obviously, the symbolic image graph $G_{f^{[n]}}$ with $n > 1$ differs from G_f. More precisely, $G_{f^{[n]}}$ might have less edges than G_f. However, $G_{f^{[n]}}$ is still useful for investigations. In order to clarify this, we introduce some theorems about the relations of f^n and f with regard to invariant sets.

Proposition 191. [9] *If $Q \subset M$ is an invariant set for f, then also for any f^n, $n \in N$, i. e.*

$$f(Q) = Q \Rightarrow f^n(Q) = Q.$$

Considering this result, we can conclude that all invariant sets of a dynamical system generated by f can also be found in a dynamical system generated by f^n.

Proposition 192. [9] *If $Q' \subset M$ is an invariant set for f^n, $n \in N$ then $Q = \bigcup_{0 \le k < n} f^k(Q')$ is an invariant set for f, i.e.*

$$f^n(Q') = Q' \Rightarrow \bigcup_{0 \le k < n} f^k(Q') = Q = f(Q).$$

Proposition 193. [9] *If $Q' \subset M$ is an invariant set for f^n, $n \in N$ then there is an invariant set Q for f with $Q' \subseteq Q$, i.e.*

$$f^n(Q') = Q' \Rightarrow \exists Q \supseteq Q' : f(Q) = Q.$$

An important conclusion of Proposition 193 is that a dynamical system generated by f^n still consists of the same invariant sets than the one generated by f. Each invariant set Q' found for f^n belongs to an invariant set Q of f. Furthermore, according to Proposition 191, all sets Q of f can be found in the dynamical system of f^n.

Recall now that most of our investigations aim to detect specific types of invariant sets. If all invariant sets of f are preserved in the dynamical system of f^n then, obviously, they can also be detected in $G_{f^{[n]}}$. However, note that the characteristics of the sets might change. Let us look, for instance, on the invariant sets of periodic points $P(p)$. The invariant set $P(6)$ of f is then equivalent to the invariant set $P(2)$ of f^3 but the points belonging to these sets have a different periodicity with respect to f and f^3. Hence, one has to be careful when analyzing the results of $G_{f^{[n]}}$. However, although the periodicity might change, every periodic point of f is also periodic for f^n, and no other periodic points than for f are found for f^n. The same is true for points belonging to quasiperiodic trajectories (without proof).

Each edge in the graph $G_{f^{[n]}}$ represents a longer part of a trajectory than in G_f. In terms of tuning this is of interest because transient dynamics can then be better distinguished from asymptotic ones. Less cells which do not contain a solution are selected for subdivision, and the growth rate of cells during the subdivision process is lower. However, the tuning has also some drawbacks. First of all, the computation time for the construction of $G_{f^{[n]}}$ increases by factor n in comparison to G_f. Furthermore, it is more likely that unstable parts of the solution, e.g. unstable periodic or quasiperiodic points, might not be detected because the forward iterates $\mathbf{y} = f^n(\mathbf{x})$ diverges stronger from these objects than $\mathbf{y} = f(\mathbf{x})$, see also the discussion in Sect. B.6.2. Last but not least, taking the analytical point of view, one must be aware about the change of characteristics regarding the invariant sets of $G_{f^{[n]}}$ in G_f.

B.6.2 Reconstruction of Fragmented Solutions

In the former sections we have discussed the usage of higher iterated functions. In many calculations, this option turned out to be an adequate technique to tune investigation methods. However, it was also mentioned that unstable parts of a solution might not be detected if the number of iterations n or the time t is chosen too large. In practice, we observed, that for crucial settings of the parameters, some unstable invariant sets do not completely disappear at once, but rather more fall apart. Some parts of them are still recognized while others vanish, as it can be seen, for instance, in Fig. B.6(a) in case of a computation of the chain recurrent set for the Lorenz system.

Such a phenomenon is a result of taking only a limited number of scan points per box in combination with following a relatively long run of trajectories in order to construct the edges of the symbolic image graph. This leads to a loss of information about the structure of unstable invariant sets. It is not our intention to give here a detailed analysis of this problem, but rather more a solution for the reconstruction of such unstable objects. Nevertheless, one should keep in mind that not every structure that looks like a disappearing unstable invariant set is necessarily a fragment of the solution. In some cases, it turned out that objects which seemed to be parts of unstable limit

cycles belonged to non-cyclic orbits. So, after the application of the method of reconstruction, further tests have to be applied to approve the correctness of obtained results.

The method, as introduced here, aims only on the reconstruction of the chain recurrent set. For other investigations, slight changes might be necessary. The reconstruction can be done by application of an extension to the symbolic image construction algorithm. The basic idea here is to add and/or select all cells belonging to boxes $M(\mathrm{i})$ of the symbolic image $G_{f^{[n]}}$ which will be passed by the forward iterates $f^1(\mathbf{x}), \ldots, f^{n-1}(\mathbf{x})$ on its way from $\mathbf{x}$ to its image $\mathbf{y} = f^n$. Therefore, first the symbolic image $G_{f^{[n]}}$ will be constructed according to the standard approach. Then the investigation method is applied in order to get the set of recurrent cells $RV(G_{f^{[n]}})$. Afterwards, the following extension must be applied before the next subdivision. For every recurrent cell $c_I \in RV(G_{f^{[n]}})$ its corresponding box $M(\mathrm{i})$ is detected. Then, for every scan point $\mathbf{x} \in S(\mathrm{i})$ it has to be checked, whether its target point $f^n(\mathbf{x}) = \mathbf{y} \in \tilde{T}(\mathrm{i})$ lies in a selected cell which is equivalent, i.e. belongs to the same set of strongly connected components. If so, we locate for each value $f^k(\mathbf{x})$, $k = 1, \ldots, (n-1)$, the box $f^k \in M(\mathrm{i}')$. If the box $M(\mathrm{i}')$ and its corresponding cell c'_{i} do not exist for a visited area, they will be added to the symbolic image. Furthermore, the cell c'_I will be marked as recurrent, no matter if it already existed or was just added.

If this extension is applied, the course of a trajectory, which connects recurrent cells, will be reconstructed. Note that the symbolic image can only become more precise by this extension. If a source cell c_i and its target cell c'_i are recurrent and equivalent, then, consequently, all the cells corresponding to boxes which are passed by the connecting trajectory are also recurrent. In fact, if all numerically computed symbolic images of an investigation would have been exact and no approximation, reconstruction would not change them. As already mentioned, this operation might add new cells to the symbolic image. So it can still be applied in a stage of subdivision when the fragmented invariant set has already fallen apart to a large extent. This can be seen in Fig. B.6(b), where unstable limit cycles of the Lorenz system are reconstructed.

B.7 Numerical Case Studies

In order to demonstrate the capabilities of symbolic analysis we present some typical examples of global analysis. The main aim hereby is to demonstrate what kind of results can be obtained with the basic investigation techniques presented in Sect. B.2, and how the parameters of the method have to be adjusted for specific investigation tasks. Also, the application of the extensions and tunings is shown. As examples we chose systems discrete as well as continuous in time. The reference machine for all these calculations was an

`Asus L3000D` laptop with an `AMD Athlon XP-M 1400+` processor and `512MB SDRAM`.

B.7.1 Ikeda Map

We start with a 2-dimensional map, namely the Ikeda map [13]. The system is defined as

$$\mathbf{x}(n+1) = f_I(\mathbf{x}(n)), \tag{B.31}$$

$f_I(\mathbf{x}) = (r + a\,(x\,\cos g(x,y) - y\,\sin g(x,y)), b\,(x\,\sin g(x,y) + y\,\cos g(x,y)))$ with $g(x,y) = c_1 - \frac{c_2}{1+x^2+y^2}$.

The numerical simulations have been carried out for the parameter values $a = b = 0.9$, $c_1 = 0.4$, $c_2 = 6.0$ and $r = 0.9$.

We start the global analysis of the system by localization of the chain recurrent set. As already mentioned, the chain recurrent set contains all kind of return trajectories and, hence, should give an overview about the areas of interest for further investigation. We set the area of investigation in the domain space to $M = [-5.0; 5.0] \times [-5.0; 5.0]$. This area M is initially divided into a covering C^0 of 20×20 boxes. Then the symbolic image G^0 is constructed for C^0. We apply the Tarjan algorithm, see Sect. B.2.1, to detect the recurrent cells. The construction and cell detection process was repeated for 4 subdivisions. In each step the boxes are subdivided into 4×4 new smaller boxes. After four subdivision steps, the distinct features of the Ikeda mapping can be found in the different recurrent sets of the symbolic image. Three areas in the state space are detected. One of them represents the stable point, the other one the unstable saddle point, and the last one contains all cells representing the chaotic attractor. It is worth mentioning that chaotic attractors can be found by computation of the chain recurrent set because their skeleton is typically build up from unstable periodic cycles [5, 6] and, therefore, recurrent points. The calculation of the symbolic image takes less than 2 minutes. In Table B.1 the number of cells in the symbolic image and the number of located recurrent cells for every subdivision level are shown. We observe that the number

Table B.1. Ikeda system: Computation of the recurrent cells. The number s marks the level of subdivision. The phase space discretization of the area $M = [-5.0; 5.0] \times [-5.0; 5.0]$ is shown. Furthermore, the number of cells belonging to a symbolic image, $|V(G^s)|$, and the number of localized recurrent cells $|RV(G^s)|$

Subdivision level s	Phase space discretization	$\lvert V(G^s)\rvert$	$\lvert RV(G^s)\rvert$
0	20×20	400	79
1	80×80	1 264	415
2	320×320	6 640	3 018
3	$1\,280 \times 1\,280$	48 288	27 878
4	$5\,120 \times 5\,120$	446 048	284 727

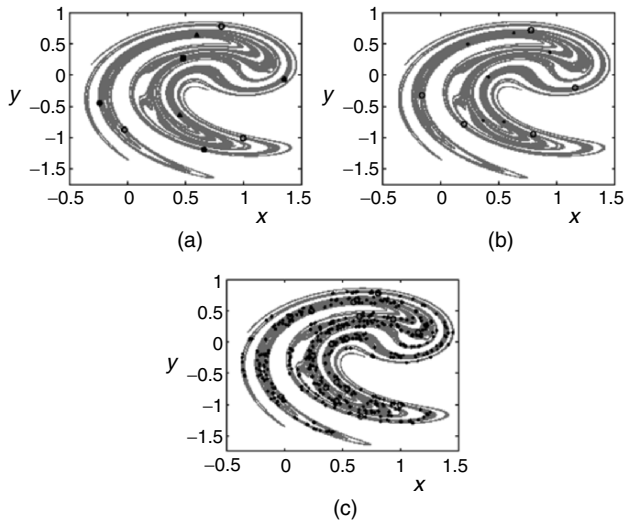

Fig. B.1. Ikeda system: (a) A fixed point (square), 2-periodic (triangles) and the two period-3 orbits (empty and filled circles). (b) Some detected unstable limit cycles with periods 5 (empty circles) and 6 (points). (c) All detected unstable 6-periodic (empty circles) and 13-periodic (points) points. Note that the chaotic attractor $\mathcal{A}$ in the background is visible for better orientation but was not calculated by the same computation

of recurrent cells grows during the subdivision process by factor ≈ 10. This high growth rate is due to the fact that it depends on the dimension of those objects which are the subject of localization, see also [14,19]. In this case, one of the subjects of localization is the chaotic attractor which has a dimension close to 2.

Our next target is the localization of periodic points. This requires, of course, the usage of the time consuming variant of the cell location algorithm based on the Dijkstra algorithm, see Sect. B.2.2. We took the same area of investigation, $M = [-5.0; 5.0] \times [-5.0; 5.0]$, than for the last computation but select only the cells with period size $p' < p = 3$ for further subdivisions. After an initial subdivision of M into 20×20 boxes, the boxes get subdivided into 8×8 new smaller boxes in every subdivision. The construction and cell detection process was repeated for 9 subdivisions. The results of the calculation in the area $[-1.5; 2.5] \times [-1.5; 2.0]$ can be seen in Fig. B.1(a), namely three fixed points, a period-2 and two period-3 orbits. It turns out that the usage of a sufficient number of scan points is important. In this example, every box contained 8×8 scan points scattered over the box, four more points close to the box corners and another one in the center. Such a high number is needed to acquire all the periodic orbits. If less scan points are chosen, another parameter must be set for error tolerance, see Sect. B.5.2, or some of the periodic cycles will not be detected. Although this calculation uses the more time consuming

period detection algorithm, the computation takes less than 30 seconds on the reference machine. This is due to the fact that only very few cells have a period size smaller or equal than 3. In our calculations, not more than 97 cells per subdivision step fit to this criterion. So the size of the symbolic images can be kept very small. However, one should notice that the performance time can increase exponentially if the parameter p is set to a higher value and more such cycles with $p' \leq p$ exist. A serious problem we come across in this computation is clustering. For most points not only one box corresponding to a periodic cell is found, but several boxes in the neighborhood. In this case we get up to 5 boxes as an outer covering for each periodic point instead of one box.

Theoretically, the following accuracy, compare Sect. B.4, could be achieved for the calculated points:

$$\epsilon \leq \frac{1}{20} \cdot \frac{1}{8^9} \cdot 4 \approx 2 \cdot 10^{-9}. \tag{B.32}$$

However, in practice, the error is higher because of clustering. If taking this into account and analyzing the computed results, the error increases to $\epsilon \leq 1 \cdot 10^{-7}$. One can expect to find in the vicinity of the chaotic attractor some unstable limit cycles with periods higher than 3. So first we increased p to 6 and then to 14. Some results of these calculations are presented in Fig. B.1(b), which shows two of the detected unstable 5- and 6-periodic orbits, and Fig. B.1(c), an overview of all detected 6- and 13-periodic points. Remarkably, the symbolic images for $p = 6$ contained not more than 325 cells, for which the corresponding boxes got subdivided and thus the calculation did not take much more computation time than in the first case ($\approx$ 30 seconds). But the location of cells with a period size ≤ 14 consisted of up to 27 000 selected cells. Boxes corresponding to each of them get subdivided into 8×8 new smaller boxes, so that the symbolic images had up to 1 700 000 cells. Therefore, the calculation took around eight hours in this case.

Until now we investigated the Ikeda system for fixed parameter values, as described above. Using the methods of symbolic analysis under variation of some parameters, interesting results can be obtained as well. For instance, one can observe the bifurcations which causes the emergence of unstable periodic orbits. These periodic orbits determine the structure of the chaotic attractor discussed above. Performing this task, we consider the area $M = [-0.4; 1.5] \times [-1.7; 1]$ in the state space and calculate the periodic orbits up to period six. Using an initial subdivision into 20×20 boxes and performing 4 subdivision steps, whereby each box is divided into $2 \times 8 \times 8$ smaller boxes, we obtain the results shown in Fig. B.2. The parameter a is varied in the interval $[0; 0.9]$. The other parameters are kept fixed to the same values as above. In this experiment we observe a period doubling bifurcation scenario and a large number of saddle-node bifurcations.

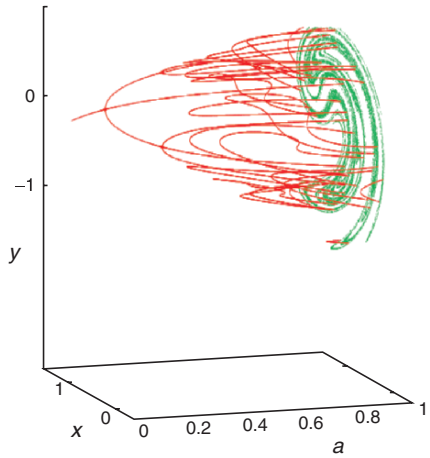

Fig. B.2. Ikeda system: Periodical points up to period 6 under variation of parameter a

B.7.2 Coupled Logistic Map

We take a look at another 2-dimensional map, the coupled logistic map defined by:

$$\mathbf{x}(n+1) = f_C(\mathbf{x}(n)), \tag{B.33}$$

$$f_C(\mathbf{x}) = ((1-r)\ g(x,a) + r\ g(y,b), r\ g(x,a) + (1-r)\ g(y,b) \tag{B.34}$$

with $\quad g(x,m) = m\ x\ (1-x)$.

The system, as presented here, can be considered as a 2-dimensional case study of coupled map lattices [16] for the logistic map [10]. For all our investigations, we fixed the parameter settings to $a = b = 3.8$ and $r = 0.07$. Analytically, it is easy to show that, due to $a = b$, we have symmetric behavior with respect to the diagonal $y = x$. This means that orbits become symmetric if one interchanges the x- and y-coordinates, and that all points on the diagonal at $y = x$ form an invariant set $\mathcal{D}$. By numerical analysis based on forward iterations and calculation of Lyapunov exponents, one can find out, that the system is governed by a single attractor $\mathcal{A}$ which consists of two symmetric parts in the phase space, see Fig. B.3(a).

Our first investigation of the system by symbolic image analysis was the computation of the chain recurrent set. We initially divided the area $M = [0.0; 1.0] \times [0.0; 1.0]$ into 5×5 boxes. In each subdivision step, a box gets divided into 3×3 new ones. After 5 subdivisions the outer covering of the chain recurrent set consists of 430 000 boxes with a side length $\approx 1 \cdot 10^{-3}$. It is important to mention that a high number of scan points is required. If taken too little, large parts of the chain recurrent set get lost during the first subdivisions. Hence, for our investigation we covered each box with a regular

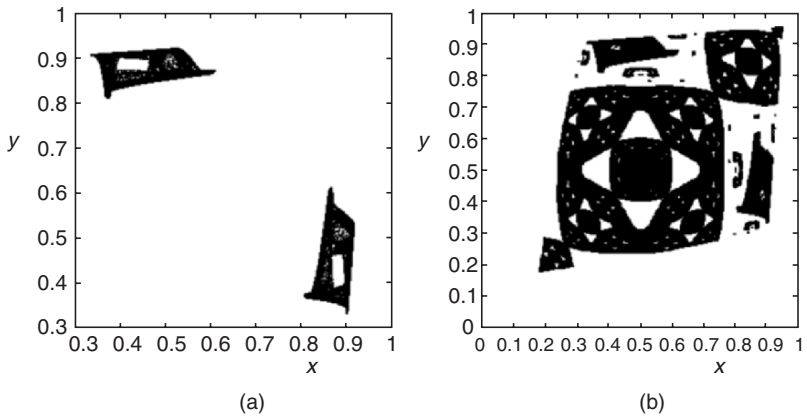

Fig. B.3. Coupled logistic map: (a) Numerical approximation of the attractor $\mathcal{A}$. (b) Numerical approximation of the chain recurrent set. One of the components is an approximation of the attractor $\mathcal{A}$

grid of 100 scan points. Applying these settings, the computation takes around 8 minutes, and its results can be seen on Fig. B.3(b). The chain recurrent set does not only consist of the chaotic attractor but also of fractal structures which are symmetric with respect to the diagonal. Note that these fractal structures are unstable entities. Orbits started in a neighborhood of the chain recurrent set are attracted by the attractor $\mathcal{A}$. We observed that even orbits started in the area covered by the computed fractal structures are attracted by $\mathcal{A}$. However, this can be explained by the fact that our numerical computation produced an outer covering of the real chain recurrent set and, hence, covers also the chain recurrent set's neighborhood. Note that the chain recurrent set consists of 4 distinct components of equivalent recurrent cell sets, one of them represents $\mathcal{A}$, and another one a 2-periodic unstable orbit in the holes of $\mathcal{A}$.

In order to verify our results, we also computed periodic orbits. We used the cell location algorithm based on the Dijkstra algorithm, see Sect. B.2.2, and computed all periodic points with a periodicity ≤ 8. We applied 17 subdivisions so that the error $\epsilon \leq 1 \cdot 10^{-8}$. The computation took around 25 minutes, and we got 614 periodic points. These points belong to periodic orbits which are scattered over the whole area designated by the approximation of the chain recurrent set. Furthermore, we checked that each of these periodic orbits is unstable.

Combining the results of our numerical computations so far, we find strong evidence for the hypothesis that the computed fractal structure of the chain recurrent set is an outer covering of a set of unstable periodic orbits of any size. This reminds us of the hypothesis of Cvitanović [5] regarding periodic orbits as the skeleton of chaotic attractors. However, the fractal structure we observe here is not an attractor.

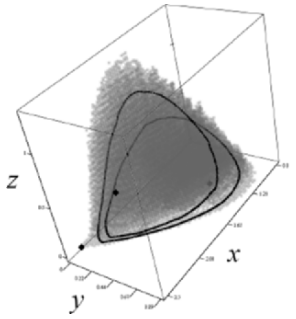

(a) second subdivision step

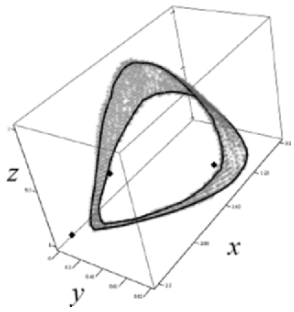

(b) third subdivision step

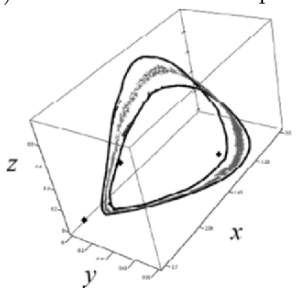

(c) fourth subdivision step

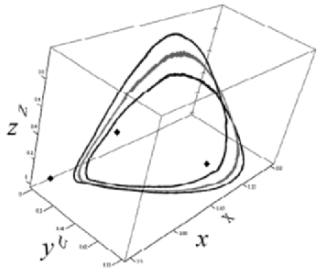

(d) tenth subdivision step

Fig. B.4. Discrete food chain model: Numerically calculated fixed points and four subdivision steps of the symbolic image construction. The outer covering of the chain recurrent set (gray), the attractor (black) and the unstable fixed points (points) are shown. The fourth fixed point at $(0, 0)$ can not be seen. Note that the attractor was separately computed by forward iterates but is also covered by the approximation of the chain recurrent set

B.7.3 Discrete Food Chain Model

Next we analyzed a discrete system of mathematical biology. The 3-dimensional dynamical model describes a discrete food chain model, studied by Lindström in [17]. The system is defined by

$$\mathbf{x}(n+1) = f_{fc}(\mathbf{x}(n)), \tag{B.35}$$

$$f_{fc}(\mathbf{x}) = \left(\frac{\mu_0\, x\, e^{-y}}{1 + x\, \max(e^{-y}, g(z)g(y))},\ \mu_1\, x\, y\, e^{-z} g(y) g(\mu_2\, y\, z),\ \mu_2\, y\, z \right)$$

$$\text{with} \quad g(s) = \begin{cases} \frac{1-e^{-s}}{s}, \text{ if } s \neq 0, \\ 1, \text{ if } s = 0. \end{cases}$$

We only focus on the following parameter setting: $\mu_0 = 3.4001$, $\mu_1 = 1$ and $\mu_2 = 4$. The analytic results of Lindström showed, that the system possesses at most four fixed points.

Our target is the computation of the chain recurrent set. We chose the area $M = [-1.0; 4.0] \times [-1.0; 4.0] \times [0.0; 1.6]$ for investigation. It turned out that it is not possible to get an appropriate approximation for the chain recurrent set by means of usual symbolic image construction. The tuning techniques must be applied to get satisfiable results. By doing so, the equilibrium points, and maybe some other information, get lost in the symbolic image after several subdivision steps. On the other hand, two invariant manifolds can be detected which belong to different components of the chain recurrent set, see Fig. B.4(d). By application of forward iteration, it can be verified that both of them consist of quasiperiodic trajectories, and that one is a stable invariant set, namely an attractor (black), while the other is an unstable invariant set (gray). Hereby, the unstable entity is not a repeller but of saddle type. For this reason, it could not be approximated by backward iterates. Such a calculation takes around one hour and the symbolic image grows up to $\approx 1\,100\,000$ cells. The long calculation time is mainly caused by the application of the tuning-techniques. Note that the localization of the unstable quasiperiodic manifold is, from the computational point of view, a nontrivial task.

In order to get a better impression how the construction process works, Fig. B.4 shows the results of several subdivision steps. Hereby, 17 scan points per box are taken. The rough position of the attractor can be located after the second subdivision of the domain space M into $200 \times 200 \times 32$ regions, see Fig. B.4(a), then, in the third subdivision, see Fig. B.4(b), the principal shape of the attractor becomes visible. But only after the fourth subdivision into $1\,200 \times 1\,200 \times 192$ regions, see Fig. B.4(c), the symbolic image splits into two different sets of equivalent recurrent cells, which correspond to the stable and unstable invariant manifolds. In order to achieve these results, it is necessary to compute the symbolic image graph for the iterated function f^{40} in the third subdivision and for f^{80} in the fourth subdivision step. Otherwise, the principal shape of the cone, see Fig. B.4(a), would persist during further subdivisions. Additionally, reconstruction of the fragmented parts must be applied in order to avoid that the cycles vanish. The final result, see Fig. B.4(d), is computed after the sixth subdivision. Note that in the subdivisions 5 and 6, also the function f^{40} is used and reconstruction of the cycles applied.

B.7.4 Lorenz System

As an example for a dynamical system continuous in time, we consider the well-known system introduced by Lorenz in [18] which is defined by

$$\begin{aligned} \dot{\mathbf{x}}(t) &= f(\mathbf{x}(t)) \\ f(\mathbf{x}) &= (\sigma(y-x),\ x(r-z)-y,\ xy-bz). \end{aligned} \tag{B.36}$$

We use the standard values of the parameters $\sigma = 10$, $b = 8/3$ and investigate the Lorenz system at two values of the parameter r, namely $r_1 \approx 14.6$ and $r_2 \approx 20$. As shown in [21], for these settings exist an unstable fixed point

$P = (0, 0, 0)^T$ and two stable ones C_1 and C_2, each of them accompanied by an unstable limit cycle. The value r_1 is chosen close to the so-called homoclinic explosion which occurs at $r \approx 13.926$, where the unstable manifolds of P return to the origin. Furthermore, at parameter value r_2, the both unstable limit cycles around C_1 and C_2 are situated close to each other and to C_1 and C_2.

In order to reproduce these results with methods of symbolic analysis, we compute the chain recurrent set. We define for r_1 and r_2 the domain spaces $M_1 = [-35.0; 35.0] \times [-35.0; 35.0] \times [0.0; 30.0]$ and $M_2 = [-20.0; 20.0] \times [-20.0; 20.0] \times [0.0; 30.0]$ as the area of investigation. The division of these spaces is initially set to $4 \times 4 \times 2$ and $2 \times 2 \times 2$ boxes. In the following subdivision stages each box is divided into $2 \times 2 \times 2$ smaller boxes. The integration step Δt is set to 0.001, and the number of iteration steps to $n_1 = 100$, $n_2 = 200$. In order to compute the integration step $\phi(\Delta t, \mathbf{x})$, the Runge-Kutta method was applied.

Figs. B.5(a) and B.5(b) show the results of the calculations for the parameters r_1 and r_2. Remarkably, one can see that the limit cycles for r_1 still touch each other, which is due to some numerical inaccuracy, while for r_2 the cycles

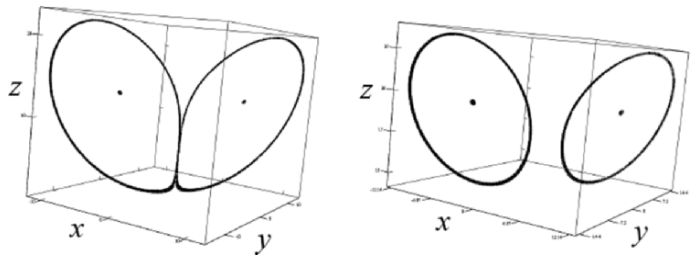

(a) $r_1 = 14.6$ (b) $r_2 = 20$

Fig. B.5. Lorenz system: Computation of an outer covering of the chain recurrent set at positions $r_1 = 14.6$ and $r_2 = 20$

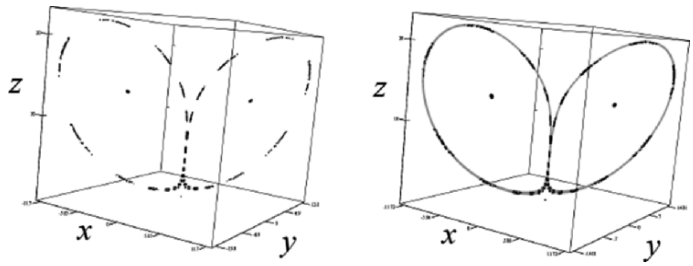

(a) before completion (b) completion of the limit cycle

Fig. B.6. Lorenz system: Reconstruction of unstable limit cycles at parameter $r_1 = 14.6$ with a large discretization time. The limit cycles fall apart and vanish by time (black), but will be completed (gray)

shrinked closer around C_1 and C_2. The computations took 30 minutes for r_1 and 2 hours for r_2. Ten subdivision steps were computed, and the symbolic images contained up to 1 400 000 cells. Hereby, the high computation time is mainly due to the relative high setting of the iteration time t. Furthermore, the unstable fixed point P can not be computed by this setting. However, if t would be set to a lower value, the limit cycles could not be detected at all because too many cells would be selected for subdivision and the memory resources would be exceeded after a few subdivisions.

The reconstruction of fragmented solutions is illustrated for the parameter setting $r_1 = 14.6$. In Fig. B.6(a) the computed approximation of the chain recurrent set after 10 subdivisions is shown. As can be seen, parts of the unstable limit cycles got lost. For this reason, the method for reconstruction of the fragmented solutions must be applied. The results are shown in Fig. B.6(b). We see that the final computation produces a precise outer covering of the unstable limit cycles.

References

1. Home page of the AnT 4.669 project, `http://www.AnT4669.de`, 2005
2. V. Avrutin, D. Fundinger, P. Levi, G.S. Osipenko, and M. Schanz, Investigation of dynamical systems using symbolic images: Efficient implementation and applications, accepted for publication by International Journal of Bifurcation and Chaos, 2005
3. V. Avrutin, R. Lammert, M. Schanz, G. Wackenhut, and G.S. Osipenko, On the software package AnT 4.669 for the investigation of dynamical systems, in *Fourth International Conference on Tools for Mathematical Modelling*, v.9, 24–35, St. Petersburg State Polytechnic University, Russia, June 2003
4. T. Cormen, C. Leiserson, and R. Rivest, *Introduction to algorithms*, The MIT electrical engineering and computer science series, MIT Press, 2000
5. P. Cvitanović, Periodic orbits as the skeleton of classical and quantum chaos, *Physica D*, 51, 1991
6. P. Cvitanović, Focus issue on periodic orbit theory, *Chaos*, 2, 1992
7. M. Dellnitz and A. Hohmann, A subdivision algorithm for the computation of unstable manifolds and global attractors, *Numerische Mathematik*, 75, 293–317, 1997
8. W. Dijkstra, A note on two problems in connection with graphs, *Numerische Math.*, 1:269–271, 1959
9. D. Fundinger, *Investigating Dynamics by Multilevel Phase Space Discretization*, PhD thesis, University of Stuttgart, 2006
10. Mat Gyllenberg, Gunnar Söderbacka, and Stefan Ericsson, Does migration stabilize local population? Analysis of a discrete metapopulation model, *Math. Biosciences*, 118, 25–49, 1993
11. S.L. Hruska, *On the numerical construction of hyperbolic structures for complex dynamical systems*, PhD thesis, Cornell University, 2002
12. C.S. Hsu, *Cell-to-Cell Mappings*. Springer, N.Y., 1987
13. K. Ikeda, Multiple-valued stationary state and its instability of the transmitted light by a ring cavity system, *Opt. Commun.*, 30, 57–261, 1979

14. O. Junge, *Mengenorientierte Methoden zur numerischen Analyse dynamischer Systeme*, PhD thesis, University of Paderbonn, 1999
15. O. Junge, Rigorous discretization of subdivision techniques, in *Proceedings of Equadiff '99, Berlin*, 2000
16. K. Kaneko, editor, *Theory and Applications of Coupled Map Lattices,* Wiley, New York, 1993
17. T. Lindström, On the dynamics of discrete food chains: Low- and high-frequency behavior and optimality of chaos, *Journal of Mathematical Biology*, 45, 396–418, 2002
18. E.N. Lorenz, Deterministic nonperiodic flow, *J. Atmos. Sci.*, 20, 130–141, 1963
19. K. Mischaikow, Topological techniques for efficient rigorous computations in dynamics, *Acta Numerica*, 2002
20. P. Pilarczyk, Computer assisted method for proving existence of periodic orbits, *TMNA*, 13(2), 365–377, 1999
21. C. Sparrow, *The Lorenz Equations: Bifurcations, Chaos, and Strange Attractors*, Springer, N.Y., 1973
22. R. Tarjan, Depth-first search and linear graph algorithms, *SIAM J. Comput*, 1, 146–160, 1972

Index

Lecture Notes in Mathematics

For information about earlier volumes
please contact your bookseller or Springer
LNM Online archive: springerlink.com

Vol. 1691: R. Bezrukavnikov, M. Finkelberg, V. Schechtman, Factorizable Sheaves and Quantum Groups (1998)
Vol. 1692: T. M. W. Eyre, Quantum Stochastic Calculus and Representations of Lie Superalgebras (1998)
Vol. 1694: A. Braides, Approximation of Free-Discontinuity Problems (1998)
Vol. 1695: D. J. Hartfiel, Markov Set-Chains (1998)
Vol. 1696: E. Bouscaren (Ed.): Model Theory and Algebraic Geometry (1998)
Vol. 1697: B. Cockburn, C. Johnson, C.-W. Shu, E. Tadmor, Advanced Numerical Approximation of Nonlinear Hyperbolic Equations. Cetraro, Italy, 1997. Editor: A. Quarteroni (1998)
Vol. 1698: M. Bhattacharjee, D. Macpherson, R. G. Möller, P. Neumann, Notes on Infinite Permutation Groups (1998)
Vol. 1699: A. Inoue,Tomita-Takesaki Theory in Algebras of Unbounded Operators (1998)
Vol. 1700: W. A. Woyczyński, Burgers-KPZ Turbulence (1998)
Vol. 1701: Ti-Jun Xiao, J. Liang, The Cauchy Problem of Higher Order Abstract Differential Equations (1998)
Vol. 1702: J. Ma, J. Yong, Forward-Backward Stochastic Differential Equations and Their Applications (1999)
Vol. 1703: R. M. Dudley, R. Norvaiša, Differentiability of Six Operators on Nonsmooth Functions and p-Variation (1999)
Vol. 1704: H. Tamanoi, Elliptic Genera and Vertex Operator Super-Algebras (1999)
Vol. 1705: I. Nikolaev, E. Zhuzhoma, Flows in 2-dimensional Manifolds (1999)
Vol. 1706: S. Yu. Pilyugin, Shadowing in Dynamical Systems (1999)
Vol. 1707: R. Pytlak, Numerical Methods for Optimal Control Problems with State Constraints (1999)
Vol. 1708: K. Zuo, Representations of Fundamental Groups of Algebraic Varieties (1999)
Vol. 1709: J. Azéma, M. Émery, M. Ledoux, M. Yor (Eds.), Séminaire de Probabilités XXXIII (1999)
Vol. 1710: M. Koecher, The Minnesota Notes on Jordan Algebras and Their Applications (1999)
Vol. 1711: W. Ricker, Operator Algebras Generated by Commuting Projećtions: A Vector Measure Approach (1999)
Vol. 1712: N. Schwartz, J. J. Madden, Semi-algebraic Function Rings and Reflectors of Partially Ordered Rings (1999)
Vol. 1713: F. Bethuel, G. Huisken, S. Müller, K. Steffen, Calculus of Variations and Geometric Evolution Problems. Cetraro, 1996. Editors: S. Hildebrandt, M. Struwe (1999)
Vol. 1714: O. Diekmann, R. Durrett, K. P. Hadeler, P. K. Maini, H. L. Smith, Mathematics Inspired by Biology. Martina Franca, 1997. Editors: V. Capasso, O. Diekmann (1999)
Vol. 1715: N. V. Krylov, M. Röckner, J. Zabczyk, Stochastic PDE's and Kolmogorov Equations in Infinite Dimensions. Cetraro, 1998. Editor: G. Da Prato (1999)
Vol. 1716: J. Coates, R. Greenberg, K. A. Ribet, K. Rubin, Arithmetic Theory of Elliptic Curves. Cetraro, 1997. Editor: C. Viola (1999)
Vol. 1717: J. Bertoin, F. Martinelli, Y. Peres, Lectures on Probability Theory and Statistics. Saint-Flour, 1997. Editor: P. Bernard (1999)
Vol. 1718: A. Eberle, Uniqueness and Non-Uniqueness of Semigroups Generated by Singular Diffusion Operators (1999)
Vol. 1719: K. R. Meyer, Periodic Solutions of the N-Body Problem (1999)
Vol. 1720: D. Elworthy, Y. Le Jan, X-M. Li, On the Geometry of Diffusion Operators and Stochastic Flows (1999)
Vol. 1721: A. Iarrobino, V. Kanev, Power Sums, Gorenstein Algebras, and Determinantal Loci (1999)
Vol. 1722: R. McCutcheon, Elemental Methods in Ergodic Ramsey Theory (1999)
Vol. 1723: J. P. Croisille, C. Lebeau, Diffraction by an Immersed Elastic Wedge (1999)
Vol. 1724: V. N. Kolokoltsov, Semiclassical Analysis for Diffusions and Stochastic Processes (2000)
Vol. 1725: D. A. Wolf-Gladrow, Lattice-Gas Cellular Automata and Lattice Boltzmann Models (2000)
Vol. 1726: V. Marić, Regular Variation and Differential Equations (2000)
Vol. 1727: P. Kravanja M. Van Barel, Computing the Zeros of Analytic Functions (2000)
Vol. 1728: K. Gatermann Computer Algebra Methods for Equivariant Dynamical Systems (2000)
Vol. 1729: J. Azéma, M. Émery, M. Ledoux, M. Yor (Eds.) Séminaire de Probabilités XXXIV (2000)
Vol. 1730: S. Graf, H. Luschgy, Foundations of Quantization for Probability Distributions (2000)
Vol. 1731: T. Hsu, Quilts: Central Extensions, Braid Actions, and Finite Groups (2000)
Vol. 1732: K. Keller, Invariant Factors, Julia Equivalences and the (Abstract) Mandelbrot Set (2000)
Vol. 1733: K. Ritter, Average-Case Analysis of Numerical Problems (2000)
Vol. 1734: M. Espedal, A. Fasano, A. Mikelić, Filtration in Porous Media and Industrial Applications. Cetraro 1998. Editor: A. Fasano. 2000.
Vol. 1735: D. Yafaev, Scattering Theory: Some Old and New Problems (2000)
Vol. 1736: B. O. Turesson, Nonlinear Potential Theory and Weighted Sobolev Spaces (2000)
Vol. 1737: S. Wakabayashi, Classical Microlocal Analysis in the Space of Hyperfunctions (2000)
Vol. 1738: M. Émery, A. Nemirovski, D. Voiculescu, Lectures on Probability Theory and Statistics (2000)
Vol. 1739: R. Burkard, P. Deuflhard, A. Jameson, J.-L. Lions, G. Strang, Computational Mathematics Driven by Industrial Problems. Martina Franca, 1999. Editors: V. Capasso, H. Engl, J. Periaux (2000)

Vol. 1740: B. Kawohl, O. Pironneau, L. Tartar, J.-P. Zolesio, Optimal Shape Design. Tróia, Portugal 1999. Editors: A. Cellina, A. Ornelas (2000)
Vol. 1741: E. Lombardi, Oscillatory Integrals and Phenomena Beyond all Algebraic Orders (2000)
Vol. 1742: A. Unterberger, Quantization and Nonholomorphic Modular Forms (2000)
Vol. 1743: L. Habermann, Riemannian Metrics of Constant Mass and Moduli Spaces of Conformal Structures (2000)
Vol. 1744: M. Kunze, Non-Smooth Dynamical Systems (2000)
Vol. 1745: V. D. Milman, G. Schechtman (Eds.), Geometric Aspects of Functional Analysis. Israel Seminar 1999-2000 (2000)
Vol. 1746: A. Degtyarev, I. Itenberg, V. Kharlamov, Real Enriques Surfaces (2000)
Vol. 1747: L. W. Christensen, Gorenstein Dimensions (2000)
Vol. 1748: M. Ruzicka, Electrorheological Fluids: Modeling and Mathematical Theory (2001)
Vol. 1749: M. Fuchs, G. Seregin, Variational Methods for Problems from Plasticity Theory and for Generalized Newtonian Fluids (2001)
Vol. 1750: B. Conrad, Grothendieck Duality and Base Change (2001)
Vol. 1751: N. J. Cutland, Loeb Measures in Practice: Recent Advances (2001)
Vol. 1752: Y. V. Nesterenko, P. Philippon, Introduction to Algebraic Independence Theory (2001)
Vol. 1753: A. I. Bobenko, U. Eitner, Painlevé Equations in the Differential Geometry of Surfaces (2001)
Vol. 1754: W. Bertram, The Geometry of Jordan and Lie Structures (2001)
Vol. 1755: J. Azéma, M. Émery, M. Ledoux, M. Yor (Eds.), Séminaire de Probabilités XXXV (2001)
Vol. 1756: P. E. Zhidkov, Korteweg de Vries and Nonlinear Schrödinger Equations: Qualitative Theory (2001)
Vol. 1757: R. R. Phelps, Lectures on Choquet's Theorem (2001)
Vol. 1758: N. Monod, Continuous Bounded Cohomology of Locally Compact Groups (2001)
Vol. 1759: Y. Abe, K. Kopfermann, Toroidal Groups (2001)
Vol. 1760: D. Filipović, Consistency Problems for Heath-Jarrow-Morton Interest Rate Models (2001)
Vol. 1761: C. Adelmann, The Decomposition of Primes in Torsion Point Fields (2001)
Vol. 1762: S. Cerrai, Second Order PDE's in Finite and Infinite Dimension (2001)
Vol. 1763: J.-L. Loday, A. Frabetti, F. Chapoton, F. Goichot, Dialgebras and Related Operads (2001)
Vol. 1764: A. Cannas da Silva, Lectures on Symplectic Geometry (2001)
Vol. 1765: T. Kerler, V. V. Lyubashenko, Non-Semisimple Topological Quantum Field Theories for 3-Manifolds with Corners (2001)
Vol. 1766: H. Hennion, L. Hervé, Limit Theorems for Markov Chains and Stochastic Properties of Dynamical Systems by Quasi-Compactness (2001)
Vol. 1767: J. Xiao, Holomorphic Q Classes (2001)
Vol. 1768: M.J. Pflaum, Analytic and Geometric Study of Stratified Spaces (2001)
Vol. 1769: M. Alberich-Carramiñana, Geometry of the Plane Cremona Maps (2002)
Vol. 1770: H. Gluesing-Luerssen, Linear Delay-Differential Systems with Commensurate Delays: An Algebraic Approach (2002)
Vol. 1771: M. Émery, M. Yor (Eds.), Séminaire de Probabilités 1967-1980. A Selection in Martingale Theory (2002)
Vol. 1772: F. Burstall, D. Ferus, K. Leschke, F. Pedit, U. Pinkall, Conformal Geometry of Surfaces in S^4 (2002)
Vol. 1773: Z. Arad, M. Muzychuk, Standard Integral Table Algebras Generated by a Non-real Element of Small Degree (2002)
Vol. 1774: V. Runde, Lectures on Amenability (2002)
Vol. 1775: W. H. Meeks, A. Ros, H. Rosenberg, The Global Theory of Minimal Surfaces in Flat Spaces. Martina Franca 1999. Editor: G. P. Pirola (2002)
Vol. 1776: K. Behrend, C. Gomez, V. Tarasov, G. Tian, Quantum Comohology. Cetraro 1997. Editors: P. de Bartolomeis, B. Dubrovin, C. Reina (2002)
Vol. 1777: E. García-Río, D. N. Kupeli, R. Vázquez-Lorenzo, Osserman Manifolds in Semi-Riemannian Geometry (2002)
Vol. 1778: H. Kiechle, Theory of K-Loops (2002)
Vol. 1779: I. Chueshov, Monotone Random Systems (2002)
Vol. 1780: J. H. Bruinier, Borcherds Products on O(2,1) and Chern Classes of Heegner Divisors (2002)
Vol. 1781: E. Bolthausen, E. Perkins, A. van der Vaart, Lectures on Probability Theory and Statistics. Ecole d' Eté de Probabilités de Saint-Flour XXIX-1999. Editor: P. Bernard (2002)
Vol. 1782: C.-H. Chu, A. T.-M. Lau, Harmonic Functions on Groups and Fourier Algebras (2002)
Vol. 1783: L. Grüne, Asymptotic Behavior of Dynamical and Control Systems under Perturbation and Discretization (2002)
Vol. 1784: L.H. Eliasson, S. B. Kuksin, S. Marmi, J.-C. Yoccoz, Dynamical Systems and Small Divisors. Cetraro, Italy 1998. Editors: S. Marmi, J.-C. Yoccoz (2002)
Vol. 1785: J. Arias de Reyna, Pointwise Convergence of Fourier Series (2002)
Vol. 1786: S. D. Cutkosky, Monomialization of Morphisms from 3-Folds to Surfaces (2002)
Vol. 1787: S. Caenepeel, G. Militaru, S. Zhu, Frobenius and Separable Functors for Generalized Module Categories and Nonlinear Equations (2002)
Vol. 1788: A. Vasil'ev, Moduli of Families of Curves for Conformal and Quasiconformal Mappings (2002)
Vol. 1789: Y. Sommerhäuser, Yetter-Drinfel'd Hopf algebras over groups of prime order (2002)
Vol. 1790: X. Zhan, Matrix Inequalities (2002)
Vol. 1791: M. Knebusch, D. Zhang, Manis Valuations and Prüfer Extensions I: A new Chapter in Commutative Algebra (2002)
Vol. 1792: D. D. Ang, R. Gorenflo, V. K. Le, D. D. Trong, Moment Theory and Some Inverse Problems in Potential Theory and Heat Conduction (2002)
Vol. 1793: J. Cortés Monforte, Geometric, Control and Numerical Aspects of Nonholonomic Systems (2002)
Vol. 1794: N. Pytheas Fogg, Substitution in Dynamics, Arithmetics and Combinatorics. Editors: V. Berthé, S. Ferenczi, C. Mauduit, A. Siegel (2002)
Vol. 1795: H. Li, Filtered-Graded Transfer in Using Noncommutative Gröbner Bases (2002)
Vol. 1796: J.M. Melenk, hp-Finite Element Methods for Singular Perturbations (2002)
Vol. 1797: B. Schmidt, Characters and Cyclotomic Fields in Finite Geometry (2002)

Vol. 1798: W.M. Oliva, Geometric Mechanics (2002)
Vol. 1799: H. Pajot, Analytic Capacity, Rectifiability, Menger Curvature and the Cauchy Integral (2002)
Vol. 1800: O. Gabber, L. Ramero, Almost Ring Theory (2003)
Vol. 1801: J. Azéma, M. Émery, M. Ledoux, M. Yor (Eds.), Séminaire de Probabilités XXXVI (2003)
Vol. 1802: V. Capasso, E. Merzbach, B.G. Ivanoff, M. Dozzi, R. Dalang, T. Mountford, Topics in Spatial Stochastic Processes. Martina Franca, Italy 2001. Editor: E. Merzbach (2003)
Vol. 1803: G. Dolzmann, Variational Methods for Crystalline Microstructure – Analysis and Computation (2003)
Vol. 1804: I. Cherednik, Ya. Markov, R. Howe, G. Lusztig, Iwahori-Hecke Algebras and their Representation Theory. Martina Franca, Italy 1999. Editors: V. Baldoni, D. Barbasch (2003)
Vol. 1805: F. Cao, Geometric Curve Evolution and Image Processing (2003)
Vol. 1806: H. Broer, I. Hoveijn. G. Lunther, G. Vegter, Bifurcations in Hamiltonian Systems. Computing Singularities by Gröbner Bases (2003)
Vol. 1807: V. D. Milman, G. Schechtman (Eds.), Geometric Aspects of Functional Analysis. Israel Seminar 2000-2002 (2003)
Vol. 1808: W. Schindler, Measures with Symmetry Properties (2003)
Vol. 1809: O. Steinbach, Stability Estimates for Hybrid Coupled Domain Decomposition Methods (2003)
Vol. 1810: J. Wengenroth, Derived Functors in Functional Analysis (2003)
Vol. 1811: J. Stevens, Deformations of Singularities (2003)
Vol. 1812: L. Ambrosio, K. Deckelnick, G. Dziuk, M. Mimura, V. A. Solonnikov, H. M. Soner, Mathematical Aspects of Evolving Interfaces. Madeira, Funchal, Portugal 2000. Editors: P. Colli, J. F. Rodrigues (2003)
Vol. 1813: L. Ambrosio, L. A. Caffarelli, Y. Brenier, G. Buttazzo, C. Villani, Optimal Transportation and its Applications. Martina Franca, Italy 2001. Editors: L. A. Caffarelli, S. Salsa (2003)
Vol. 1814: P. Bank, F. Baudoin, H. Föllmer, L.C.G. Rogers, M. Soner, N. Touzi, Paris-Princeton Lectures on Mathematical Finance 2002 (2003)
Vol. 1815: A. M. Vershik (Ed.), Asymptotic Combinatorics with Applications to Mathematical Physics. St. Petersburg, Russia 2001 (2003)
Vol. 1816: S. Albeverio, W. Schachermayer, M. Talagrand, Lectures on Probability Theory and Statistics. Ecole d'Eté de Probabilités de Saint-Flour XXX-2000. Editor: P. Bernard (2003)
Vol. 1817: E. Koelink, W. Van Assche(Eds.), Orthogonal Polynomials and Special Functions. Leuven 2002 (2003)
Vol. 1818: M. Bildhauer, Convex Variational Problems with Linear, nearly Linear and/or Anisotropic Growth Conditions (2003)
Vol. 1819: D. Masser, Yu. V. Nesterenko, H. P. Schlickewei, W. M. Schmidt, M. Waldschmidt, Diophantine Approximation. Cetraro, Italy 2000. Editors: F. Amoroso, U. Zannier (2003)
Vol. 1820: F. Hiai, H. Kosaki, Means of Hilbert Space Operators (2003)
Vol. 1821: S. Teufel, Adiabatic Perturbation Theory in Quantum Dynamics (2003)
Vol. 1822: S.-N. Chow, R. Conti, R. Johnson, J. Mallet-Paret, R. Nussbaum, Dynamical Systems. Cetraro, Italy 2000. Editors: J. W. Macki, P. Zecca (2003)
Vol. 1823: A. M. Anile, W. Allegretto, C. Ringhofer, Mathematical Problems in Semiconductor Physics. Cetraro, Italy 1998. Editor: A. M. Anile (2003)
Vol. 1824: J. A. Navarro González, J. B. Sancho de Salas, $\mathscr{C}^\infty$ – Differentiable Spaces (2003)
Vol. 1825: J. H. Bramble, A. Cohen, W. Dahmen, Multiscale Problems and Methods in Numerical Simulations, Martina Franca, Italy 2001. Editor: C. Canuto (2003)
Vol. 1826: K. Dohmen, Improved Bonferroni Inequalities via Abstract Tubes. Inequalities and Identities of Inclusion-Exclusion Type. VIII, 113 p, 2003.
Vol. 1827: K. M. Pilgrim, Combinations of Complex Dynamical Systems. IX, 118 p, 2003.
Vol. 1828: D. J. Green, Gröbner Bases and the Computation of Group Cohomology. XII, 138 p, 2003.
Vol. 1829: E. Altman, B. Gaujal, A. Hordijk, Discrete-Event Control of Stochastic Networks: Multimodularity and Regularity. XIV, 313 p, 2003.
Vol. 1830: M. I. Gil', Operator Functions and Localization of Spectra. XIV, 256 p, 2003.
Vol. 1831: A. Connes, J. Cuntz, E. Guentner, N. Higson, J. E. Kaminker, Noncommutative Geometry, Martina Franca, Italy 2002. Editors: S. Doplicher, L. Longo (2004)
Vol. 1832: J. Azéma, M. Émery, M. Ledoux, M. Yor (Eds.), Séminaire de Probabilités XXXVII (2003)
Vol. 1833: D.-Q. Jiang, M. Qian, M.-P. Qian, Mathematical Theory of Nonequilibrium Steady States. On the Frontier of Probability and Dynamical Systems. IX, 280 p, 2004.
Vol. 1834: Yo. Yomdin, G. Comte, Tame Geometry with Application in Smooth Analysis. VIII, 186 p, 2004.
Vol. 1835: O.T. Izhboldin, B. Kahn, N.A. Karpenko, A. Vishik, Geometric Methods in the Algebraic Theory of Quadratic Forms. Summer School, Lens, 2000. Editor: J.-P. Tignol (2004)
Vol. 1836: C. Năstăsescu, F. Van Oystaeyen, Methods of Graded Rings. XIII, 304 p, 2004.
Vol. 1837: S. Tavaré, O. Zeitouni, Lectures on Probability Theory and Statistics. Ecole d'Eté de Probabilités de Saint-Flour XXXI-2001. Editor: J. Picard (2004)
Vol. 1838: A.J. Ganesh, N.W. O'Connell, D.J. Wischik, Big Queues. XII, 254 p, 2004.
Vol. 1839: R. Gohm, Noncommutative Stationary Processes. VIII, 170 p, 2004.
Vol. 1840: B. Tsirelson, W. Werner, Lectures on Probability Theory and Statistics. Ecole d'Eté de Probabilités de Saint-Flour XXXII-2002. Editor: J. Picard (2004)
Vol. 1841: W. Reichel, Uniqueness Theorems for Variational Problems by the Method of Transformation Groups (2004)
Vol. 1842: T. Johnsen, A.L. Knutsen, K3 Projective Models in Scrolls (2004)
Vol. 1843: B. Jefferies, Spectral Properties of Noncommuting Operators (2004)
Vol. 1844: K.F. Siburg, The Principle of Least Action in Geometry and Dynamics (2004)
Vol. 1845: Min Ho Lee, Mixed Automorphic Forms, Torus Bundles, and Jacobi Forms (2004)
Vol. 1846: H. Ammari, H. Kang, Reconstruction of Small Inhomogeneities from Boundary Measurements (2004)
Vol. 1847: T.R. Bielecki, T. Björk, M. Jeanblanc, M. Rutkowski, J.A. Scheinkman, W. Xiong, Paris-Princeton Lectures on Mathematical Finance 2003 (2004)
Vol. 1848: M. Abate, J. E. Fornaess, X. Huang, J. P. Rosay, A. Tumanov, Real Methods in Complex and CR Geometry, Martina Franca, Italy 2002. Editors: D. Zaitsev, G. Zampieri (2004)

Vol. 1849: Martin L. Brown, Heegner Modules and Elliptic Curves (2004)
Vol. 1850: V. D. Milman, G. Schechtman (Eds.), Geometric Aspects of Functional Analysis. Israel Seminar 2002-2003 (2004)
Vol. 1851: O. Catoni, Statistical Learning Theory and Stochastic Optimization (2004)
Vol. 1852: A.S. Kechris, B.D. Miller, Topics in Orbit Equivalence (2004)
Vol. 1853: Ch. Favre, M. Jonsson, The Valuative Tree (2004)
Vol. 1854: O. Saeki, Topology of Singular Fibers of Differential Maps (2004)
Vol. 1855: G. Da Prato, P.C. Kunstmann, I. Lasiecka, A. Lunardi, R. Schnaubelt, L. Weis, Functional Analytic Methods for Evolution Equations. Editors: M. Iannelli, R. Nagel, S. Piazzera (2004)
Vol. 1856: K. Back, T.R. Bielecki, C. Hipp, S. Peng, W. Schachermayer, Stochastic Methods in Finance, Bressanone/Brixen, Italy, 2003. Editors: M. Fritelli, W. Runggaldier (2004)
Vol. 1857: M. Émery, M. Ledoux, M. Yor (Eds.), Séminaire de Probabilités XXXVIII (2005)
Vol. 1858: A.S. Cherny, H.-J. Engelbert, Singular Stochastic Differential Equations (2005)
Vol. 1859: E. Letellier, Fourier Transforms of Invariant Functions on Finite Reductive Lie Algebras (2005)
Vol. 1860: A. Borisyuk, G.B. Ermentrout, A. Friedman, D. Terman, Tutorials in Mathematical Biosciences I. Mathematical Neurosciences (2005)
Vol. 1861: G. Benettin, J. Henrard, S. Kuksin, Hamiltonian Dynamics – Theory and Applications, Cetraro, Italy, 1999. Editor: A. Giorgilli (2005)
Vol. 1862: B. Helffer, F. Nier, Hypoelliptic Estimates and Spectral Theory for Fokker-Planck Operators and Witten Laplacians (2005)
Vol. 1863: H. Fürh, Abstract Harmonic Analysis of Continuous Wavelet Transforms (2005)
Vol. 1864: K. Efstathiou, Metamorphoses of Hamiltonian Systems with Symmetries (2005)
Vol. 1865: D. Applebaum, B.V. R. Bhat, J. Kustermans, J. M. Lindsay, Quantum Independent Increment Processes I. From Classical Probability to Quantum Stochastic Calculus. Editors: M. Schürmann, U. Franz (2005)
Vol. 1866: O.E. Barndorff-Nielsen, U. Franz, R. Gohm, B. Kümmerer, S. Thorbjønsen, Quantum Independent Increment Processes II. Structure of Quantum Levy Processes, Classical Probability, and Physics. Editors: M. Schürmann, U. Franz, (2005)
Vol. 1867: J. Sneyd (Ed.), Tutorials in Mathematical Biosciences II. Mathematical Modeling of Calcium Dynamics and Signal Transduction. (2005)
Vol. 1868: J. Jorgenson, S. Lang, $\mathrm{Pos}_n(\mathrm{R})$ and Eisenstein Sereies. (2005)
Vol. 1869: A. Dembo, T. Funaki, Lectures on Probability Theory and Statistics. Ecole d'Eté de Probabilités de Saint-Flour XXXIII-2003. Editor: J. Picard (2005)
Vol. 1870: V.I. Gurariy, W. Lusky, Geometry of Müntz Spaces and Related Questions. (2005)
Vol. 1871: P. Constantin, G. Gallavotti, A.V. Kazhikhov, Y. Meyer, S. Ukai, Mathematical Foundation of Turbulent Viscous Flows, Martina Franca, Italy, 2003. Editors: M. Cannone, T. Miyakawa (2006)
Vol. 1872: A. Friedman (Ed.), Tutorials in Mathematical Biosciences III. Cell Cycle, Proliferation, and Cancer (2006)
Vol. 1873: R. Mansuy, M. Yor, Random Times and Enlargements of Filtrations in a Brownian Setting (2006)
Vol. 1874: M. Yor, M. Andr Meyer - S minaire de Probabilités XXXIX (2006)
Vol. 1875: J. Pitman, Combinatorial Stochastic Processes. Ecole dŠEté de Probabilités de Saint-Flour XXXII-2002. Editor: J. Picard (2006)
Vol. 1876: H. Herrlich, Axiom of Choice (2006)
Vol. 1877: J. Steuding, Value Distributions of L-Functions(2006)
Vol. 1878: R. Cerf, The Wulff Crystal in Ising and Percolation Models, Ecole d'Et de Probabilits de Saint-Flour XXXIV-2004. Editor: Jean Picard (2006)
Vol. 1879: G. Slade, The Lace Expansion and its Appli- cations, Ecole d'Eté de Probabilités de Saint-Flour XXXIV-2004. Editor: Jean Picard (2006)
Vol. 1880: S. Attal, A. Joye, C.-A. Pillet, Open Quantum Systems I, The Hamiltonian Approach (2006)
Vol. 1881: S. Attal, A. Joye, C.-A. Pillet, Open Quantum Systems II, The Markovian Approach (2006)
Vol. 1882: S. Attal, A. Joye, C.-A. Pillet, Open Quantum Systems III, Recent Developments (2006)
Vol. 1883: W. Van Assche, F. Marcell n (Eds.), Orthogonal Polynomials and Special Functions, Computation and Application (2006)
Vol. 1884: N. Hayashi, E.I. Kaikina, P.I. Naumkin, I.A. Shishmarev, Asymptotics for Dissipative Nonlinear Equations (2006)
Vol. 1885: A. Telcs, The Art of Random Walks (2006)
Vol. 1886: S. Takamura, Splitting Deformations of Degenerations of Complex Curves (2006)
Vol. 1887: K. Habermann, L. Habermann, Introduction to Symplectic Dirac Operators (2006)
Vol. 1888: J. van der Hoeven, Transseries and Real Differential Algebra (2006)
Vol. 1889: G. Osipenko, Dynamical Systems, Graphs, and Algorithms (2007)

Recent Reprints and New Editions

Vol. 1618: G. Pisier, Similarity Problems and Completely Bounded Maps. 1995 – Second, Expanded Edition (2001)
Vol. 1629: J.D. Moore, Lectures on Seiberg-Witten Invariants. 1997 – Second Edition (2001)
Vol. 1638: P. Vanhaecke, Integrable Systems in the realm of Algebraic Geometry. 1996 – Second Edition (2001)
Vol. 1702: J. Ma, J. Yong, Forward-Backward Stochastic Differential Equations and their Applications. 1999. – Corrected 3rd printing (2005)